NASA Technical Memorandum 107690

RIGID BODY MODE IDENTIFICATION OF THE PAH-2 HELICOPTER USING THE EIGENSYSTEM REALIZATION ALGORITHM

Axel Schenk and Richard S. Pappa

October 1992

National Aeronautics and Space Administration

Langley Research Center
Hampton, Virginia 23665

Rigid Body Mode Identification of the PAH-2 Helicopter Using the Eigensystem Realization Algorithm

Axel Schenk and Richard S. Pappa

Summary

The rigid body modes of the PAH-2 'TIGER' helicopter were identified using the Eigensystem Realization Algorithm (ERA). This work complements ground vibration tests performed using DLR's traditional phase resonance technique and ISSPA. Rigid body modal parameters are important for ground resonance prediction. Time-domain data for ERA were obtained by inverse Fourier transformation of frequency response functions measured with stepped-sine excitation. Mode purity (based on the Phase Resonance Criterion) was generally equal to or greater than corresponding results obtained in the ground vibration tests. All identified natural frequencies and mode shapes correlate well with corresponding ground vibration test results.

The modal identification approach discussed in this report has become increasingly attractive in recent years due to the steadily declining cost and increased performance of scientific computers. As illustrated in this application modern time-domain methods can be successfully applied to data acquired using DLR's existing test equipment. Some suggestions are made for future applications of time domain modal identification in this manner.

Acronyms

APS	Average Power Spectrum (equation 1)
ATWL	Analysis Time Window Length
CMI	Consistent Mode Indicator (ERA's primary accuracy indicator)
DLR	Deutsche Forschungsanstalt für Luft- und Raumfahrt e.V.
EMAC	Extended Modal Amplitude Coherence
ERA	Eigensystem Realization Algorithm
FRF	Frequency Response Function
GVT	Ground Vibration Test
IRF	Impulse Response Function
ISSPA	Identification of Structural System Parameters (method)
MAC	Modal Assurance Criterion (mode shape correlation measure) (equation 4)
MBB	Messerschmitt-Bölkow-Blohm GmbH, a division of Deutsche Aerospace
MIF	Mode Indicator Function (equation 2)
PAH	Panzer Abwehr Hubschrauber (anti-tank helicopter)
PRC	Phase Resonance Criterion (equation 3)
PRM	Phase Resonance Method

1. Introduction

In January 1991, ground vibration tests were performed by DLR on the first prototype of the Franco-German PAH-2 'TIGER' helicopter [1] at the MBB site in Ottobrunn, Germany [2]. Test objectives were identification of structural dynamic characteristics (modal parameters) and measurement of transmissibilities (frequency response functions). Among several issues of helicopter dynamics, the ground resonance problem is of great significance. Ground resonance is a dynamic instability involving the coupling of the rotor blade lag motion with the in-plane motion of the rotor hub [3]. When in contact with the ground, the critical structural mode is usually a rigid body oscillation of the helicopter on its landing gear. Ground resonance instability is avoided by having sufficiently-low rigid body natural frequencies and/or adequate damping.

As a complement to the ground vibration tests conducted using DLR's traditional phase resonance technique [4] and ISSPA [5,6], some post-test time domain analyses were also performed in August 1991. The rigid body modes were selected as the target of this work because frequency response functions were available from [2], and as a contribution to the prediction of ground resonance behavior. Time domain data (specifically, impulse response functions) were derived from the measured frequency response functions using an inverse fast Fourier transformation.

In this report the application and results of the time domain analysis are presented. The Eigensystem Realization Algorithm (ERA) [7-9] was used for modal parameter identification. Recently, a comparison of results obtained with the phase resonance method (sinusoidal excitation with appropriated forces) and with ERA (multiple-input analysis of directly measured free-decay time histories) has shown that these dissimilar methods both yield reliable modal parameters of high correlation [10]. Correlation of results provides increased confidence in difficult testing situations.

The modal identification approach discussed in this report has become increasingly attractive in recent years due to the steadily declining cost and increased performance of scientific computers. As illustrated in this application, modern time-domain methods can be successfully applied to data acquired using DLR's existing large test facility. No additional tests are necessary by using frequency response functions acquired during initial sweep runs.

2. Test Article

Figure 1 shows a photograph of the test setup. During the tests the helicopter was standing on the ground and was configured as follows:

- no main rotor blades,
- no tail rotor blades,
- no mast mounted sight,

- with dummy masses for horizontal stabilizer end plates,
- with normal shock absorber pressure,
- with normal tire pressure,
- with pilot and gunner dummy masses (2 × 110 kg),
- with fuel (1088 kg), and
- with dummy stubwing stores (480 kg).

The gross weight during testing was approximately 4600 kg and was measured by means of a force transducer. The overall dimensions of the structure are:

- length : 15.03 m,
- height : 5.09 m,
- width : 4.34 m.

3. Data Acquisition and Assessment

Five sets of frequency response functions (FRFs) were available for analysis. The parameters of each data set are listed in **Table 1**. The corresponding exciter locations are shown in **Figure 2**. These FRF data were measured using stepped-sine excitation and converted into digitally filtered (bandlimited) time histories using an inverse Fourier transformation. Each set of resulting impulse response functions (IRFs) consists of 242 acceleration histories. Because of the inconsistent frequency ranges and number of data points of the various tests, each data set is analyzed separately in a single-input, multiple-output analysis.

Representative FRFs and corresponding IRFs are shown in **Figures 3 through 7**. These data were measured on the horizontal stabilizer in the x, y, and z directions, respectively, going from top to bottom in each figure. The noise level is very low based on the smoothness of the FRF curves. Low noise, of course, simplifies data analysis. However, several characteristics which complicate data analysis are also seen. First, nonlinear behavior (unsymmetrical response peaks) is observed, for instance, for the mode near 2.4 Hz in Record 183 of Figure 4. This observation correlates with the discussion of nonlinearities in [2], associated primarily with the actions of the wheels and landing gear. Secondly, spurious data spikes occur near 4.9 Hz in all three FRFs in Figure 6. These "gain peaks" occurred when sensor amplifiers were switched to avoid overloads near resonance. Thirdly, more than six response peaks occur in some FRFs, for example, in Record 183 of Figure 3. However, only the six rigid body modes are known to occur in this frequency interval. A fourth data irregularity is observed in Record 183 of Figure 3 in the frequency interval from 4.6 Hz to 6.0 Hz. No explanation can be given for the unusually-flat, large magnitude function seen here.

The transformation of bandlimited FRFs into IRFs calculates a fictitious sampling frequency based on the frequency range of the FRFs. Therefore, the data oscillation frequencies observed in the IRFs of Figures 3 through 7 are distorted. The damping rates, however, are unaffected by the transformation. Using Record 181

of Figure 3 as an example, this distortion is explained as follows. The first peak in the FRF occurs at approximately 0.25 Hz after the initially measured frequency of 1.4 Hz. The associated cycle time is computed as the reciprocal of 0.25 Hz or 4.0 sec. This cycle time is observed in the IRF for the dominant oscillation. However, the correct frequency for this peak is, in fact, 1.65 Hz, corresponding to a cycle time of 0.61 sec. During analysis, this distorsion is eliminated by adding the initially measured frequency to the frequency results. This is a standard feature of ERA. With bandlimited FRFs, the sampling frequency of the IRF equals twice the bandwidth of the corresponding FRF. Similarly, the number of time samples in the IRF equals twice the number of frequency lines in the FRF.

As an overview of all 242 FRF measurements, **Figures 8 through 12** show average power spectra (APS) and mode indicator functions (MIFs) for each of the five data sets. These functions are calculated as follows:

$$APS\,(f) = \frac{\sum_{i=1}^{n_p} | u_i\,(f) |^2}{n_p} \tag{1}$$

and

$$MIF\,(f) = \left[1.0 - \frac{\sum_{i=1}^{n_p} | u_i'\,(f) | \, | u_i\,(f) |}{\sum_{i=1}^{n_p} | u_i\,(f) |^2} \right] \cdot 1000 \tag{2}$$

where $u_i'\,(f)$ and $| u_i\,(f) |$ are the real part and magnitude, respectively, of the ith response measurement with respect to the applied force. n_p is the total number of physical response measurements.

Both of these functions display peaks at each natural frequency. Additionally, the APS shows the relative magnitude of each modal response. The MIF, on the other hand, provides no information concerning modal response magnitudes; however, the resolution of individual modes is much higher. As noted previously in the FRF plots, significant deviations from linear behavior (unsymmetrical response peaks) are seen in some functions, for example, for the mode near 2.5 Hz in the MIF of Figure 9. Also, the "gain peak" observed in test AFXZL1 is clearly seen as a large spike in the APS of Figure 11.

In summary, appreciable nonlinearity and other minor data irregularities are observed in the FRFs measured on the PAH-2 helicopter. Such characteristics are not uncommon in dynamics tests of large, built-up structures. These factors complicate, but do not preclude, accurate modal identification.

4. Initial Results

4.1 ERA Application Approach and Evaluation Criteria

Previous experience has shown that significant changes can occur in ERA analyses as a function of the assumed number of modes. In particular, optimum accuracy for different modes typically occurs at different numbers of assumed modes. Also, weakly excited modes often require relatively high numbers of assumed modes to be properly identified. For these reasons, the assumed number of modes is incremented in each analysis from 1 up to 15.

Reliable modal parameters, in particular the damping values, are obtained if ERA's primary accuracy indicator, the Consistent-Mode Indicator (CMI), reaches values larger than approximately 80 percent. Compared with the damping results, identified frequencies and mode shapes are typically reliable at lower CMI values. CMI measures the consistency of identified mode shape components, both temporally and spatially. Components from the beginning of the data analysis window are compared with corresponding components at the end of the window. Additionally, the spatial collinearity of mode-shape phase angles is included in the calculation. CMI is a proven, reliable accuracy indicator. A complete description is given in [11].

Normal mode purity is assessed using the well-established Phase Resonance Criterion (PRC). PRC is not a standard ERA accuracy indicator, but is used here for comparisons with DLR's traditional phase resonance testing approach. It is computed in the same manner as MIF, Eq. (2), except using the identified (complex) mode shapes instead of response measurements:

$$PRC_j = \left[1.0 - \frac{\sum_{i=1}^{n_p} | \Phi'_{ij} | \, | \Phi_{ij} |}{\sum_{i=1}^{n_p} | \Phi_{ij} |^2} \right] \cdot 1000 \qquad (3)$$

where Φ'_{ij} and $| \Phi_{ij} |$ are the real part and magnitude, respectively, of the ith component of the jth identified mode shape. Modes with PRC values greater than 950 are generally accepted as well-identified normal modes.

4.2 Frequency, Damping, Accuracy Indicators, and MAC

Initial ERA results for each of the five tests are shown in **Figures 13a through 17a**, respectively. Each figure consists of a frequency plot, a plot of the viscous damping factor (percent of critical damping), a plot of CMI (as a measure of reliability) and a plot of PRC (as a measure of normal mode purity). These results are plotted versus the assumed number of modes, varying from 1 to 15. Each row of results corresponds to a separate ERA analysis with a specified number of assumed modes.

In the frequency plot, each detected mode is represented by a vertical dash at the associated frequency. The confidence in each result is expressed by the length of the vertical dash which is proportional to CMI. The highest confidence is attained if the distance between minor tic marks on the vertical axis is filled. Thus, more confidence is associated with results appearing as solid vertical lines than with those appearing as dotted or dashed lines.

In the remaining three plots in each figure, the corresponding results for damping, CMI, and PRC are displayed using numerals for each mode appearing in the frequency plot. The parameters for the lowest frequency mode (along each row) are plotted using a "1", for the second-lowest frequency (along the same row) using a "2", and so forth. Due to the actual number of identified frequencies, the numbering of damping values and accuracy indicators of individual modes may change over successive rows.

The identified frequencies in Figures 13a through 17a are labeled with the deformation pattern based on associated mode shape results. Using the Modal Assurance Criterion (MAC) [12], each of the ERA-identified mode shapes is correlated with each of the six rigid body modes determined in the ground vibration test [2], as follows:

$$(4) \qquad MAC_{GVT/ERA} = \frac{\left| \Phi_{GVT}^{H} \Phi_{ERA} \right|^2}{\left(\Phi_{GVT}^{H} \Phi_{GVT} \right) \left(\Phi_{ERA}^{H} \Phi_{ERA} \right)}$$

where H designates the Hermitian transpose. MAC values range from 0.0 for two independent (orthogonal) vectors to 1.0 for two identical vectors (differing at most by a scale factor). Values greater than approximately 0.7 indicate a considerable degree of similarity.

These MAC results are shown in **Figures 13b through 17b** using a simple graphical format. Each row and column in these figures represents one mode shape. The value of MAC is proportional to the size of the rectangle drawn at the intersection of the corresponding row and column. MAC values greater than 0.7 are darkened for emphasis. In general, each ERA-identified mode correlates highly and uniquely with one of the six modes identified in the GVT. Each mode is labeled with three numbers. The first of which is the case number, i.e. the number of assumed modes. The second of which is the order number of the mode in the particular case. The associated frequency is also shown as the third number. Best mode shape results based on PRC from the GVT are recorded along the ordinate while all ERA mode shapes are recorded along the abscissa.

All GVT modes are decoupled from each other. Thus, mode coupling of ERA results is indicated if in the same column one ERA mode correlates with two or more GVT modes, for example in Figure 16b, case 15: ERA mode 4 with GVT modes 4 and 6. On the other hand, repeated identification of the same mode shape within the same case is also indicated if several ERA modes correlate with one GVT mode, for example in Figure 15b, case 15: ERA modes 1, 3, and 4 with GVT mode 1. Ideally, each rigid body mode should be identified only once in each case, for example in Figure 15b, yaw mode.

The initial results obtained for each test are discussed individually in the following paragraphs:

For test **AFXL1**, Figure 13, stable results in both frequency and damping are achieved for yaw, vertical, and roll modes. Stable frequency results are also obtained for the longitudinal mode; however, the corresponding damping factors show greater spread at values between 6 and 8 percent. Increasing the number of assumed modes, the pitch mode damping decreases continuously to values around 1 percent while CMI increases to approximately 50 percent. The pitch mode also shows "mode splitting" at three particular values of assumed number of modes (10, 14, and 15), attributed to nonlinearity. Note in Figure 13b that the corresponding pairs of mode shapes all show high correlation with the GVT pitch mode. With the exception of the pitch mode, best CMI results for all detected modes are higher than 80 percent and PRC values are higher than 950.

Test **AFXL2**, Figure 14, used the same exciter location as test AFXL1 (longitudinal excitation at the rotor hub) except at a higher force level (160 N vs. 140 N). Again, stable frequency and damping results are obtained for yaw, vertical, and roll modes. Due to nonlinearity, the frequencies are 25 percent (yaw), 12 percent (vertical), and 7 percent (roll) higher than the corresponding frequencies of test AFXL1. Now, best CMI values of these modes have increased to above 90 percent and PRC values to above 970. Based on mode shape correlations (Figure 14b), multiple identification of the longitudinal mode occurred in the frequency range of approximately 2 to 3 Hz. The associated damping estimates show wide variation between 2 and 7 percent. Best CMI values are approximately 80 percent. Also, PRC values higher than 950 (associated with the 2.35 Hz results) indicate good mode purity. Considering the highly unsymmetrical peak in the MIF and the high, but flat-top response in the average power spectum (Figure 9), the unusual phenomenon of multiple identification may be explained and attributed to nonlinearity. Since the measurements were limited to frequencies below 5 Hz, no pitch mode is identified in test AFXL2. The lateral mode is not detected in test AFXL2 (or AFXL1) because of the inappropriate excitation direction.

Although test **AFYL1** was performed to excite the lateral mode better (using lateral excitation at the rotor hub), surprisingly only one acceptable identification of this mode is obtained (at 14 assumed modes), see Figure 15. However, a CMI value of only 48 percent indicates relatively low confidence. At 15 assumed modes, multiple identification occurred with even lower CMI than in the previous case. Since this mode is identified all together only five times (in three cases), an evaluation of stability of modal parameters is impossible. The CMI results for the longitudinal and vertical modes are similarly low due to the inappropriate direction of excitation. On the other hand, stable frequency and damping results are obtained for both the yaw and roll modes. These modes attain CMI values above 80 percent and PRC values above 970.

The mode indicator function of test **AFXZL1**, Figure 11, shows several peaks below 3 Hz. Based on mode shape correlations, modes are extracted in this frequency range which are combinations of lateral and longitudinal, and vertical motions, coupled with pitch, see Figure 16. The corresponding damping results show a wide spread of values between 6 and 10 percent. Also, CMI as well as PRC indicate low confidence in these modes. Once again, yaw and roll modes are identified with stable frequency and damping values, and CMI values of approximately 80 percent

and PRC values above 950. The pitch mode is identified at 4.9 Hz with a best CMI value of 56 percent and a PRC value of 929. Note that this frequency coincides exactly with the "gain peak" discussed in Section 3. However, the plot of the mode indicator function, Figure 11, discloses that a response peak is at exactly 5 Hz which can be attributed to the pitch mode. Since the gain peak generally extends higher in magnitude than the true FRFs, an incorrect frequency result is apparently obtained for the pitch mode. In addition, the damping result decreases to zero with increasing assumed number of modes which is in good agreement with a narrow peak in the FRFs. Obviously, both frequency and damping results for this mode are questionable. On the other hand, high confidence can be given in the mode shape estimate because a pitch mode pattern is obtained.

Figure 17 shows the initial ERA results for test **AFXZL2**, using antisymmetric excitation at the landing gear. Low-confidence results with CMI less than 40 percent are again found for both lateral and longitudinal modes. CMI values increase to 95 percent for the yaw mode with increasing numbers of assumed modes, while for the roll mode CMI values are optimum at moderate numbers of assumed modes. Nevertheless, stable frequency and damping estimates and PRC values above 960 are obtained for both modes. A mode of low confidence (with CMI of approximately 20 percent and PRC near 800) is found at a frequency of 5.1 Hz which correlates with none of the six rigid body modes. Although the CMI values are not quite satisfactory, the pitch mode is clearly detected at 5.6 Hz, with damping and mode shape based on PRC showing stable results.

The best results for each mode based on CMI are listed in **Table 2**, together with the analysis time window length (ATWL) used in each case. Only certain modes are identified in certain tests. Also, most modes show a significant spread of frequency and damping values. This can be explained by the different excitation locations and levels used in the various tests and the nonlinear response of the structure attributed to the actions of wheels and landing gear.

In summary, four of the six rigid body modes are identified with high confidence (CMI of at least 80 percent) in the initial ERA analyses. The remaining two, the lateral and pitch modes, can only be obtained with unsatisfactory confidence. Further analyses are needed, in particular to evaluate reliable damping factors. Appreciable variations of modal parameters (frequency and damping) occurred for all six modes due to structural nonlinearities. Comparing the FRF measurements, Figures 3 through 7, with the ERA findings, Figures 13 through 17, good agreement in corresponding frequencies is seen.

4.3 Mode Shapes

Identified mode shapes from the initial analyses are plotted in **Figures 18 through 23**. Modes having the highest CMI values in Table 2 are shown. All six modes correlate to a high degree with the corresponding mode shapes identified in the GVT using the traditional phase resonance method and ISSPA. Correlation coefficients (MAC) of the GVT and initial ERA results are listed in **Table 3**.

5. Improved Results

The motivation for the improvement of results, discussed in this section, can be seen in Table 2. Most of the modes have CMI values of approximately 80 percent or higher and sufficient confidence can be placed in the associated modal parameters. On the other hand, some modes show insufficient CMI values. This low confidence in some results is also expressed by dotted or dashed frequency lines in Figures 13a through 17a, for example in Figures 15a through 17a for the lateral mode. Together with the longitudinal mode, the lateral mode is most important to the ground resonance problem. Therefore, accurate frequency and damping estimates for these modes are a major objective of the test program and, also, of the ERA analyses reported here.

5.1 Approach

Complex structures require a high number of sensors for adequate resolution and identification of all mode shapes. However, only a subset of all sensors attached to the structure is needed for identification of specific modes. Modal identification of target modes, in particular the damping estimation, can be improved if a subset of the inputs (excitation locations) and outputs (sensor locations) is emphasized which matches the requirements of the target modes. Then, unsuitable excitations and sensors with lower signal-to-noise ratios are neglected. While emphasizing the target mode, normally all other modes are de-emphasized. This secondary feature fails if the selection of key excitations and/or sensors accidently matches other modes. Each mode of interest normally requires a dedicated analysis. Successful applications of this improvement technique have been demonstrated in [9,10].

In this project, mode shape patterns for selection of key sensors are provided by the initial analyses. Ten optimal responses are used in each improvement analysis. Criteria for selection are high accuracy indicator values (EMAC) and a corresponding high modal amplitude at the location of the key sensor. EMAC, the Extended Modal Amplitude Coherence, is used in the calculation of CMI and provides information concerning the controllability and observability of the modes in terms of each individual excitation point (input) and sensor measurement (output).

A feature of ERA is that complete mode shapes are derived in analyses using key sensors. This is accomplished by retaining all response measurements in the first block row of ERA's data input matrix. In all following block rows, only the responses of the specified key sensors are included.

5.2 Results

Six results from Table 2 are selected as target modes for the improvement technique described above. CMI values of

- lateral mode Tests AFYL1 and AFXZL2;
- vertical mode Test AFYL1;

- pitch mode Tests AFXL1, AFXZL1, and AFXZL2

are below 70 percent. The associated damping values show some variation and, in particular for the lateral mode, only a few estimates were obtained in the initial analyses.

5.2.1 Lateral Mode

Improved results for the lateral mode are shown in **Figures 24 and 25** as expanded views of the frequency range from 1.0 to 2.0 Hz. Best CMI values in both analyses are now approximately 80 percent and PRC values in test AFYL1 have increased considerably to above 970. In both damping plots, some random variation is seen. However, a damping value between 6 and 12 percent is estimated with the excitation used in test AFYL1 (also in other analyses not shown here), while a damping between 10 and 15 percent is estimated with the excitation used in test AFXZL2.

The response amplitude of the lateral mode was approximately twice as large in test AFXZL2 than in test AFYL1, based on [2]. Due to nonlinearities, the natural frequency of this mode decreased from 1.44 Hz in test AFYL1 to 1.23 Hz in test AFXZL2, with a corresponding damping increase by a factor of two. These nonlinearity trends correlate closely with those reported in [2].

5.2.2 Vertical Mode

The current limitation of the improvement technique is demonstrated with the vertical mode in test AFYL1, **Figure 26**. Little improvement is possible due to the inadequacy of the excitation in this test. The best CMI value obtained is now only 56 percent and the associated PRC value is 883. This is an example where two other strongly excited modes in the vincinity of the target mode are not significantly deemphasized. The lateral excitation used in this test is more appropriate to the yaw and roll modes than to the vertical mode.

5.2.3 Pitch Mode

Expanded views of the frequency range from 4.5 to 5.8 Hz are provided in **Figures 27 through 29**, showing improved results for the pitch mode. The wide variation of frequency and damping according to different excitations used in tests AFXL1, AFXZL1 and AFXZL2 and seen in Table 2 is corroborated by the improvement results.

A good stabilization of damping results with high CMI values is achieved in tests AFXL1 and AFXZL2, while no stabilization is obtained in test AFXZL1. In the latter case, results with CMI above 50 percent have damping values between 1.0 and 2.6 percent. The low CMI values of AFXL1/14 and of AFXZL1/12 in the initial analyses are increased to values of 80 percent or higher together with some increase of PRC. Smaller accuracy improvement from 68 to 77 percent in CMI is possible in test AFXZL2; however, the corresponding PRC value decreases from 966 to 941.

5.3 Assessment

Six cases of Table 2 were selected as candidates for improvement analyses. The findings are summarized in **Tables 4 and 5**. With the exception of the vertical mode, significant improvement of accuracy based on the parameter CMI was achieved. Compared to the results shown in Table 2, more confidence can now be given in the stated modal parameters. In five of the six cases, CMI values have increased considerably. With the vertical mode, however, less improvement of CMI was achievable due to an insufficient excitation and other dominant modes at nearby frequencies.

6. Comparison of ERA and GVT Results

A comparison of ERA and GVT results is given in **Table 6**. Only modes with similar excitation are compared. Unfortunately, no damping estimates were available from [2] for these modes. Therefore, best identified modes based on PRC from the ground vibration tests are also listed and indicated with an asterisk.

Overall, there is *excellent* correlation of frequency results. As discussed earlier, the corresponding mode shapes are also highly similar. The identified damping values also show good agreement although, of course, the sparsity of results limits the usefulness of the comparison.

PRC values obtained using ERA are higher in 9 of the 10 cases than corresponding values obtained in the GVT. It must be realized that a tight time schedule during the GVT prevented additional efforts to achieve higher PRC values.

7. Conclusions

Rigid body mode identification of the PAH-2 'TIGER' helicopter was performed using the Eigensystem Realization Algorithm (ERA). This work complements the ground vibration tests performed with DLR's classical PRM approach and ISSPA. Not all modal parameters, in particular the damping values, could be evaluated reliably with PRM and ISSPA due to nonlinearities.

Five data sets with various force levels and excitation locations were analyzed with ERA. Analyses were performed in a single-input manner due to differences in data acquisition parameters among the data sets. Nevertheless, reliable results for most modes were obtained in the initial analyses. A wide variation of modal parameters was found among the separate tests due to the highly nonlinear response of the structure. For modes with low accuracy indicators, improvement analyses were successfully conducted emphasizing a subset of ten sensors of a total number of 242.

All identified frequencies and mode shapes correlate well with their counterparts of the ground vibration test [2]. PRC values obtained with ERA were equal to or greater than corresponding results obtained in the GVT.

In closing, the authors would like to make the following suggestions for improving future applications of ERA:

- *Perform ERA analyses at the test site using FRF data measured during initial PRM sweep runs.* These sweep runs are always conducted prior to tuning individual modes; however, FRFs are not normally saved during this phase of testing. Only the mode indicator function is usually evaluated. ERA-identified mode shapes would be available to assist in subsequent selection of optimum shaker locations and force distributions.

- *Use the same setup of data acquisition parameters for all tests in order to permit multiple-input ERA analyses.* In this case, further reduction of analysis time is possible. With sequential single-input analyses, mode shape correlation is needed to associate results for the same mode. This step is unnecessary with multiple-input analysis because only one result per mode is extracted as the best least-squares estimate. With highly nonlinear responses, however, multiple-input analysis may reach its limitation. If input forces and exciter locations used in the individual tests cause too great a variation of structural response and accordingly shifts in modal parameters, single-input analysis may be preferable (or multiple-input analysis with a reduced number of selected inputs).

- *Begin sweep runs at a frequency sufficiently less than the lowest frequency of interest.* Sweep runs which begin too close to a mode of interest, for example, the mode at 1.5 Hz in Record 182 of Figure 3, cause too great a distortion on the corresponding IRF for accurate modal identification, in particular for the damping value.

- *Minimize data acquisition time by using unequally spaced frequency lines.* A minimum of five data points should be measured in the half-power bandwidth of each resonance, but the number of data points acquired between resonances can be much less.

8. Bibliography

[1] Jonda, W. and Libeer, J.-P.: *The Franco-German Tiger Program: A Status Report.* Vertiflite, Vol. pp. 34-41.

[2] Degener, M. and Sinapius, M.: *Ground Vibration Tests on the Helicopter PAH-2 'Tiger'.* DLR IB 232 - 91 C 03, April 1991.

[3] Johnson, W.: *Helicopter Theory.* Princeton University Press, Princeton, NJ, 1980.

[4] Breitbach, E.: *A Semi-Automatic Modal Survey Test Technique for Complex Aircraft and Spacecraft Structures.* Proceedings of the 3rd ESRO Testing Symposium, Frascati, Italy, October 1973, pp. 519-528.

[5] Link, M. and Vollan, A.: *Identification of Structural System Parameters from Dynamic Response Data.* Z. Flugwiss. Weltraumforsch., Vol. 2, No. 3, 1978, pp. 165-174.

[6] Link, M.: *Theory of a Method for Identifying Incomplete System Matrices from Vibration Test Data.* Z. Flugwiss. Weltraumforsch., Vol. 9, No. 2, 1985, pp. 76-82.

[7] Juang, J.-N. and Pappa, R.S.: *An Eigensystem Realization Algorithm for Modal Parameter Identification and Model Reduction.* Journal of Guidance, Control, and Dynamics, Vol. 8, No. 5, September-October 1985, pp. 620-627.

[8] Juang, J.-N. and Pappa, R.S.: *Effects of Noise on Modal Parameters Identified by the Eigensystem Realization Algorithm.* Journal of Guidance, Control, and Dynamics, Vol. 9, No. 3, May-June 1986, pp. 294-303.

[9] Pappa, R.S., Schenk, A., and Noll, C.: *ERA Modal Identification Experiences with Mini-Mast.* Proceedings of the 2nd USAF/NASA Workshop on System Identification and Health Monitoring of Precision Space Structures, Pasadena, CA, USA, March 1990, pp 331-370.

[10] Pappa, R. S., Schenk, A., Niedbal, N., and Klusowski, E.: *Comparison of Two Dissimilar Modal Identification Techniques.* Proceedings of the International Forum on Aeroelasticity and Structural Dynamics 1991, Aachen, FRG, June 1991.

[11] Pappa, R. S.: *A Consistent-Mode Indicator for ERA.* To Be Presented at the AIAA Dynamics Specialists Conference, Dallas, TX, USA, April 1992.

[12] Allemang, R. J. and Brown, D. L.: *A Correlation Coefficient for Modal Vector Analysis.* Proceedings of the 1st International Modal Analysis Conference, Orlando, FL, USA, November 1982, pp. 110-116.

9. List of Tables

Table 1: Test Parameters
Table 2: Initial Identification Results
Table 3: Correlation of GVT and Initial ERA Mode Shapes
Table 4: Improved Identification Results
Table 5: Comparison of GVT and Improved ERA Mode Shapes
Table 6: Comparison of ERA Results with GVT Results from [2]

10. List of Figures

Figure 1: Test Configuration
Figure 2: Exciter Locations

Figure 3: Typical FRFs and IRFs for Test AFXL1
Figure 4: Typical FRFs and IRFs for Test AFXL2
Figure 5: Typical FRFs and IRFs for Test AFYL1
Figure 6: Typical FRFs and IRFs for Test AFXZL1
Figure 7: Typical FRFs and IRFs for Test AFXZL2

Figure 8: Avg. Power Spectrum and Mode Indicator Function for Test AFXL1
Figure 9: Avg. Power Spectrum and Mode Indicator Function for Test AFXL2
Figure 10: Avg. Power Spectrum and Mode Indicator Function for Test AFYL1
Figure 11: Avg. Power Spectrum and Mode Indicator Function for Test AFXZL1
Figure 12: Avg. Power Spectrum and Mode Indicator Function for Test AFXZL2

Figure 13a: Initial ERA Results for Test AFXL1
Figure 13b: Correlation of ERA and GVT Modes for Test AFXL1
Figure 14a: Initial ERA Results for Test AFXL2
Figure 14b: Correlation of ERA and GVT Modes for Test AFXL2
Figure 15a: Initial ERA Results for Test AFYL1
Figure 15b: Correlation of ERA and GVT Modes for Test AFYL1
Figure 16a: Initial ERA Results for Test AFXZL1
Figure 16b: Correlation of ERA and GVT Modes for Test AFXZL1
Figure 17a: Initial ERA Results for Test AFXZL2
Figure 17b: Correlation of ERA and GVT Modes for Test AFXZL2

Figure 18: Lateral Mode Shape
Figure 19: Longitudinal Mode Shape
Figure 20: Yaw Mode Shape
Figure 21: Vertical Mode Shape
Figure 22: Roll Mode Shape
Figure 23: Pitch Mode Shape

Figure 24: Improved Results for Lateral Mode (Test AFYL1)
Figure 25: Improved Results for Lateral Mode (Test AFXZL2)
Figure 26: Improved Results for Vertical Mode (Test AFYL1)
Figure 27: Improved Results for Pitch Mode (Test AFXL1)
Figure 28: Improved Results for Pitch Mode (Test AFXZL1)
Figure 29: Improved Results for Pitch Mode (Test AFXZL2)

Test	Excitation Loc./Force - / N	Frequency Range Hz	Time Samples	Time Window sec	Sampling Frequency Hz
AFXL1	E1 / 140	1.4 - 6.0	184	20.0	9.2
AFXL2	E1 / 160	1.3 - 5.0	370	50.0	7.4
AFYL1	E2 / 120	1.0 - 5.0	400	50.0	8.0
AFXZL1	E21,E22 / 500	1.0 - 6.0	500	50.0	10.0
AFXZL2	E21,E22 / ±500	1.0 - 6.0	200	20.0	10.0

Table 1. Test Parameters (Sine Sweeps)

Mode	Test/Case	Frequency Hz	Damping Factor (viscous), %	CMI %	PRC	ATWL sec
Lateral	AFYL1/14	1.22	4.50	48	934	4.457
	AFXZL2/10	1.31	11.71	36	963	4.100
Longitudinal	AFXL1/09	1.65	6.60	90	960	4.457
	AFXL2/15	2.35	2.99	78	976	5.541
Yaw	AFXL1/14	2.78	1.78	85	966	4.457
	AFXL2/14	3.48	2.27	95	973	5.541
	AFYL1/12	3.41	2.16	88	972	5.125
	AFXZL1/15	3.53	2.42	92	960	4.100
	AFXZL2/14	3.46	2.43	95	968	4.100
Vertical	AFXL1/11	3.38	2.39	83	951	4.457
	AFXL2/14	3.77	2.26	93	986	5.541
	AFYL1/13	3.81	2.30	53	861	5.125
Roll	AFXL1/15	4.00	1.11	94	977	4.457
	AFXL2/11	4.26	1.06	96	979	5.541
	AFYL1/13	3.96	1.86	89	971	5.125
	AFXZL1/12	4.02	3.12	79	972	4.100
	AFXZL2/09	3.82	4.94	83	968	4.100
Pitch	AFXL1/14	4.59	0.91	54	928	4.457
	AFXZL1/12	4.90	1.72	56	929	4.100
	AFXZL2/13	5.59	2.57	68	966	4.100

Table 2. Initial Identification Results (Best Results Based on CMI)

Mode	Mode Reference Label		MAC,
	GVT	ERA	%
Lateral	AY101	AFYL1/14	99
Longitudinal	A09L2	AFXL1/09	91
Yaw	A05L1	AFXL2/14	97
Vertical	A03L1	AFXL2/14	90
Roll	AY103	AFXL2/11	96
Pitch	A02L1	AFXZL2/13	87

Table 3. Correlation of GVT and Initial ERA Mode Shapes

Mode	Test/Case	Frequency Hz	Damping Factor (viscous), %	CMI %	PRC	ATWL sec
Lateral	AFYL1-KD4/10	1.44	7.79	78	974	2.875
	AFXZL2-KD3/14	1.23	12.55	78	964	4.100
Vertical	AFYL1-KD1/14	3.83	2.94	56	883	5.250
Pitch	AFXL1-KD5/11	4.61	0.96	85	959	7.935
	AFXZL1-KD1/12	4.90	1.96	80	943	4.100
	AFXZL2-KD4/13	5.61	2.60	77	941	4.100

Table 4. Improved Identification Results

Mode	Mode Reference Label		MAC,
	GVT	ERA	%
Lateral	AY101	AFYL1-KD4/10	99
Pitch	A02L1	AFXL1-KD5/11	93

Table 5. Correlation of GVT and Improved ERA Mode Shapes

Table 6. Comparison of ERA Results with GVT Results from [2].

Mode	Mode Reference Label		Frequency, Hz		Viscous Damping Factor, %		PRC	
	GVT	ERA	GVT	ERA	GVT	ERA	GVT	ERA
Lateral	AY101 *	AFYL1-KD4/10	1.46	1.44	-	7.79	976	974
	AXZ201	AFXZL2-KD3/14	1.30	1.23	-	12.55	930	964
Longitudinal	A10L1	AFXL1/09	1.64	1.65	-	6.60	940	960
	AX201	AFXL2/15	2.42	2.35	-	2.99	930	976
	A09L2 *	no FRFs available	1.77		3.38 $		958	
Yaw	AY102	AFYL1/12	3.44	3.41	-	2.16	803	972
	AXZ202	AFXZL2/14	3.45	3.46	-	2.43	657	968
	A05L1 *	no FRFs available	2.52		2.18 $		971	
Vertical	AX202	AFXL2/14	3.78	3.77	-	2.26	713	986
	A03L1 *	no FRFs available	3.80		1.83 $		897	
Roll	AXZ203	AFXZL2/09	3.90	3.82	-	4.94	827	968
	AY103 *	AFYL1/13	3.98	3.96	-	1.86	943	971
Pitch	AXZ102	AFXZL1-KD1/12	4.98	4.90	-	1.96	840	943
	A02L1 *	no FRFs available	5.22		2.43 $		927	

* indicates best GVT result based on PRC in [2]
$ indicates average value of several damping estimates

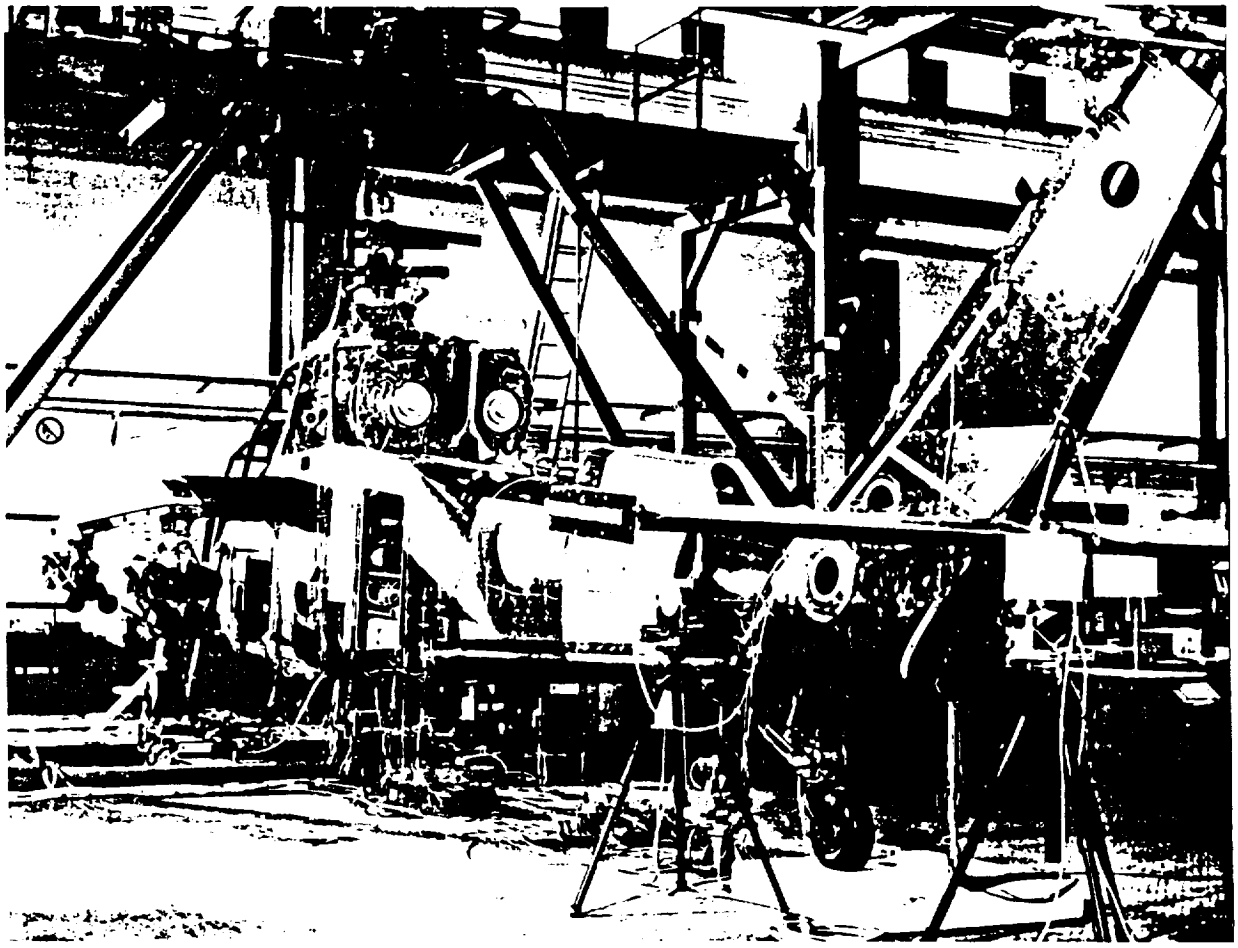

Figure 1. Test Configuration

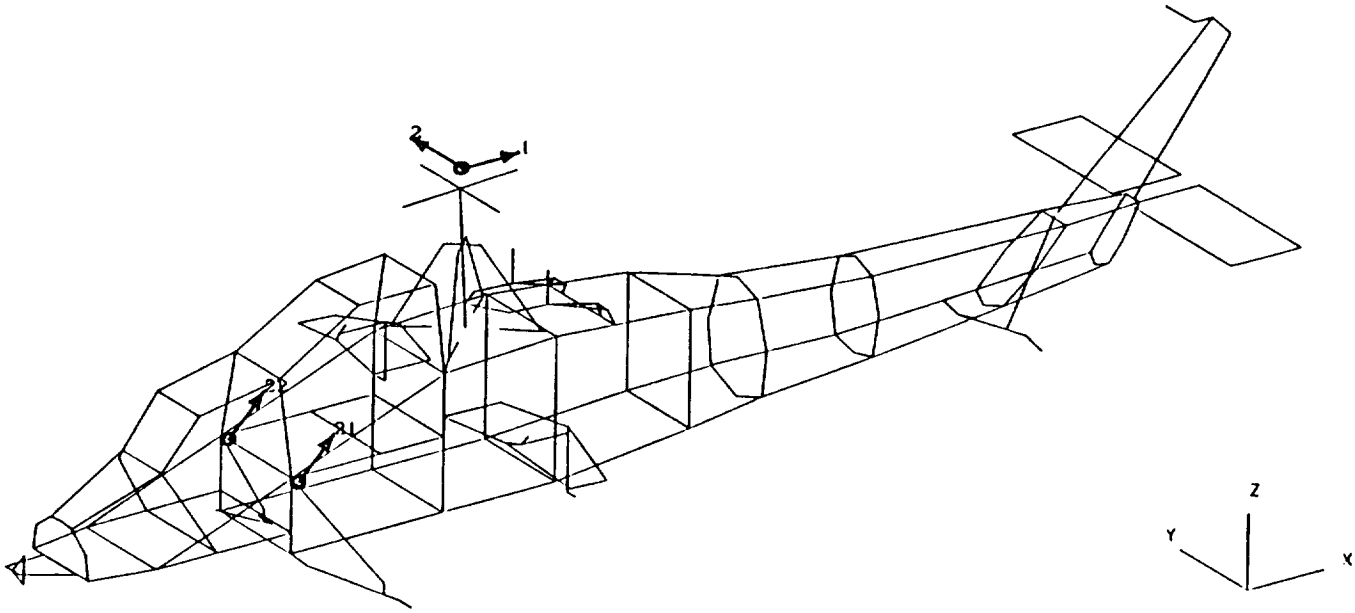

Figure 2. Exciter Locations

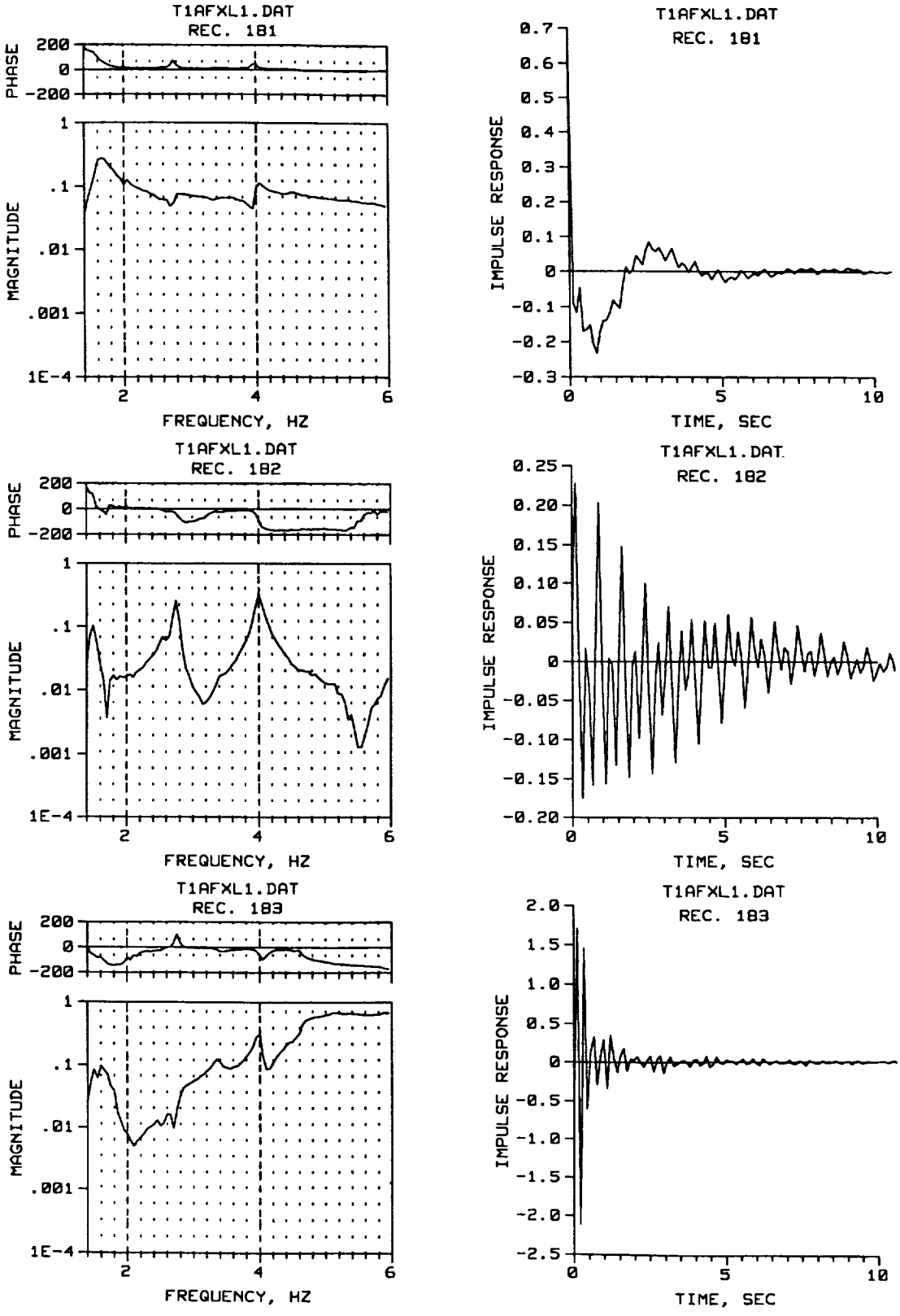

Figure 3. Typical FRFs and IRFs for Test AFXL1

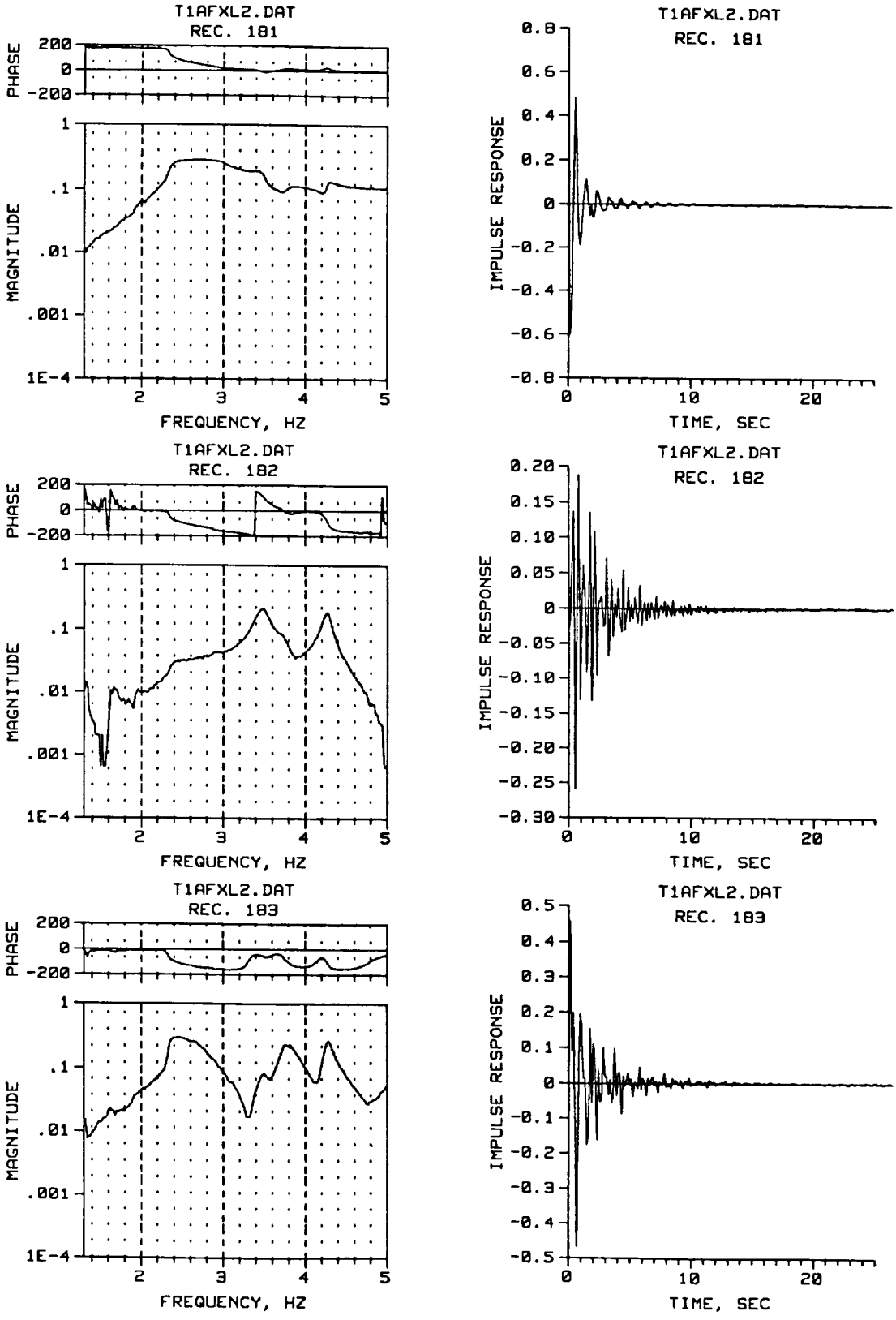

Figure 4. Typical FRFs and IRFs for Test AFXL2

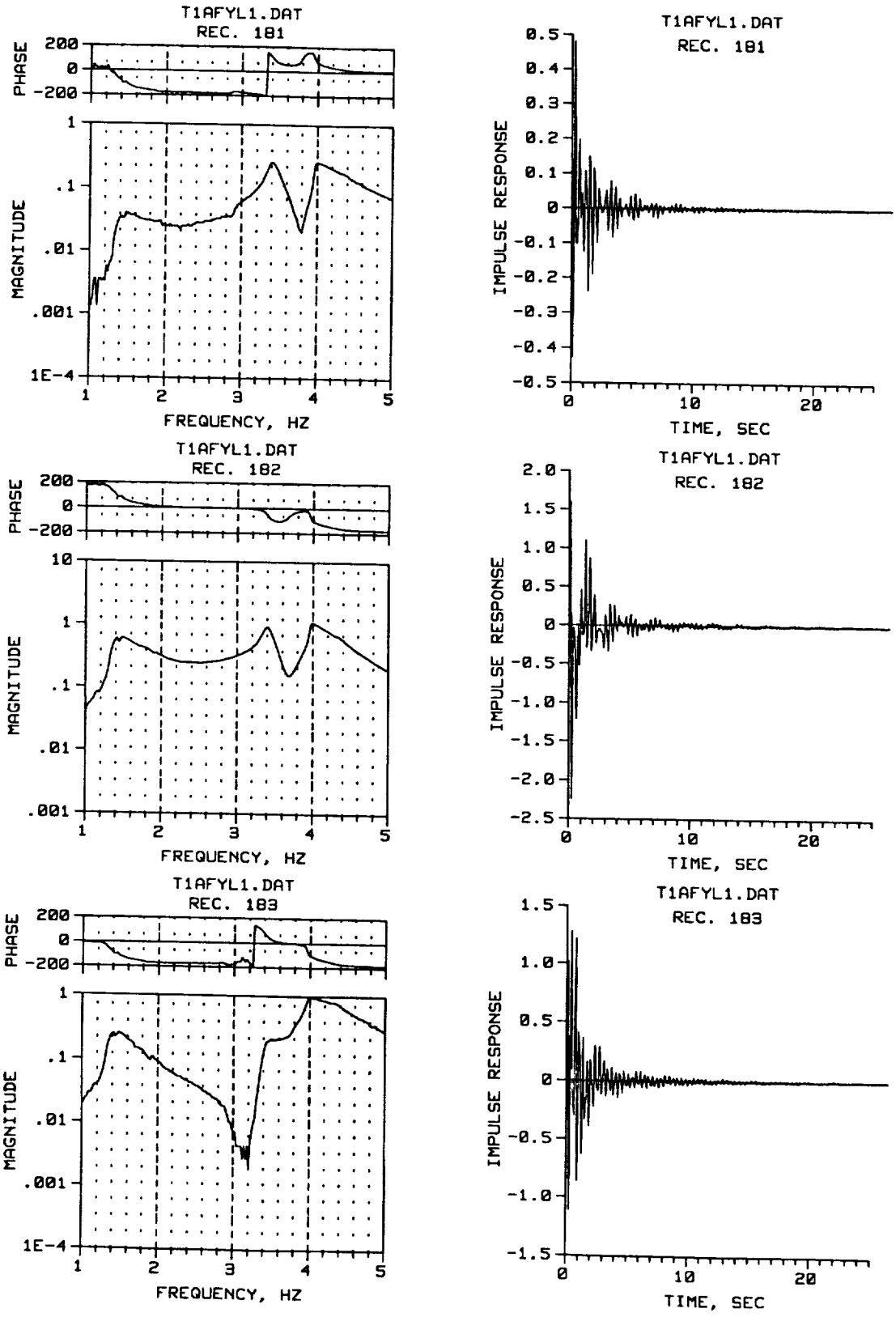

Figure 5. Typical FRFs and IRFs for Test AFYL1

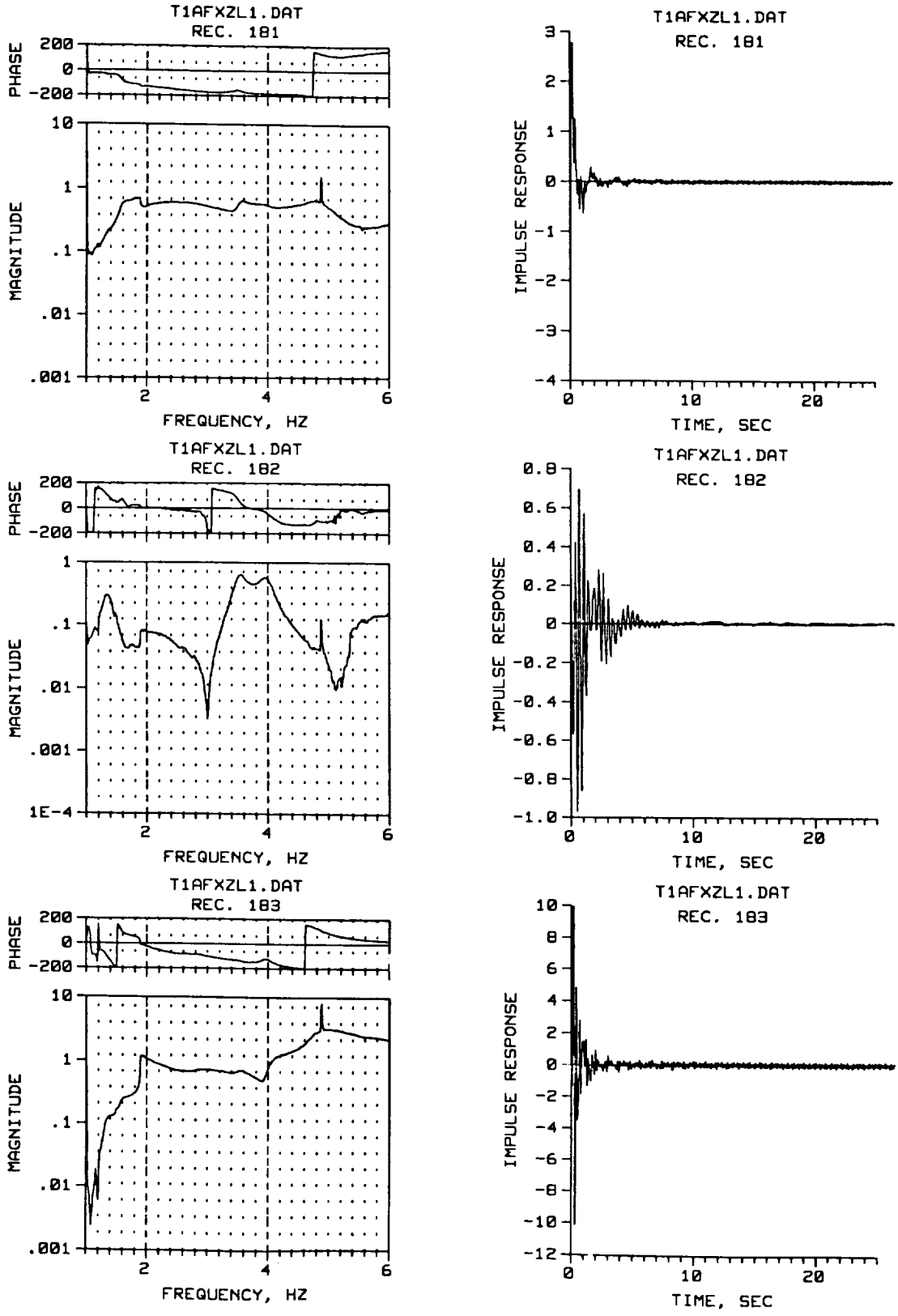

Figure 6. Typical FRFs and IRFs for Test AFXZL1

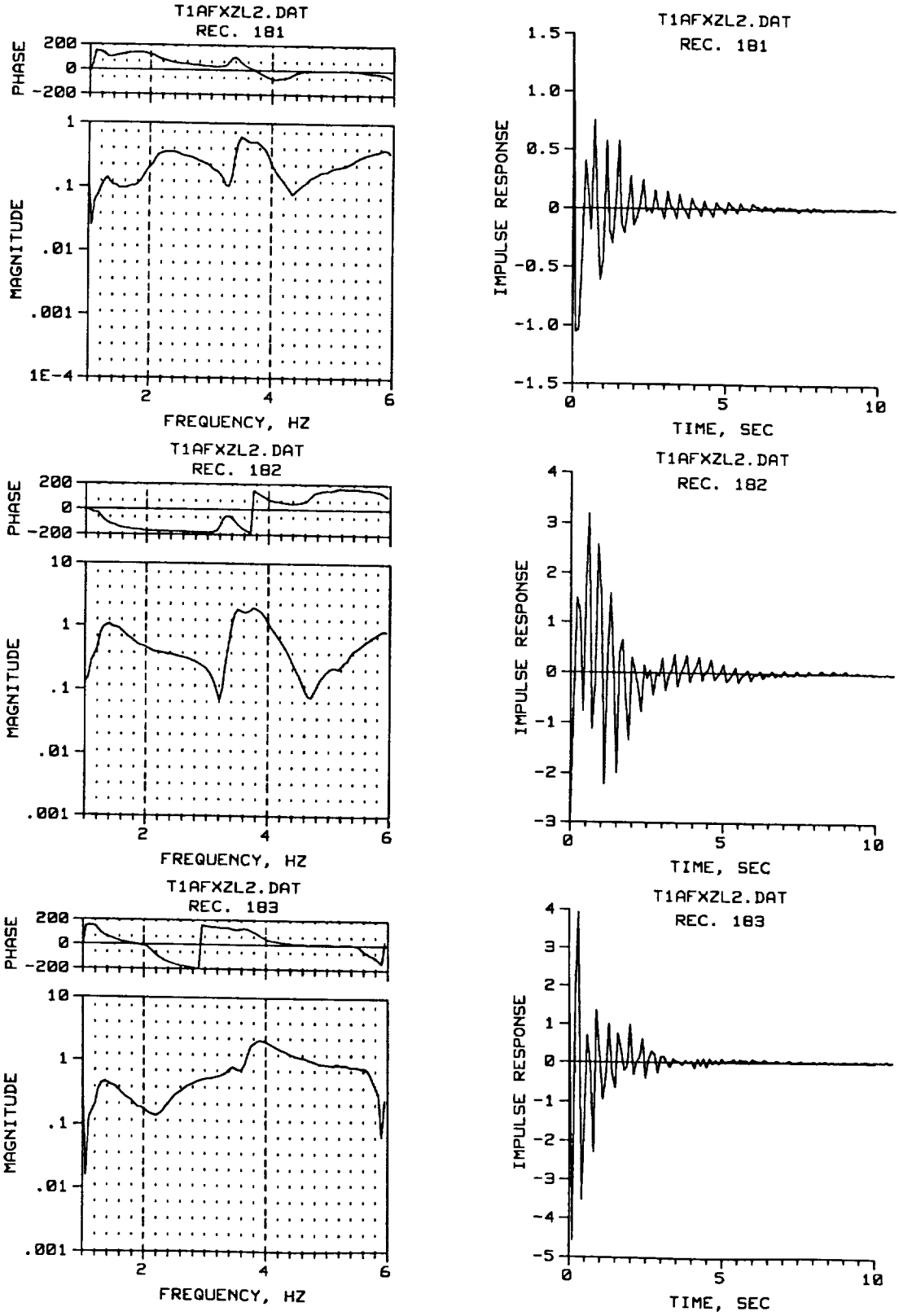

Figure 7. Typical FRFs and IRFs for Test AFXZL2

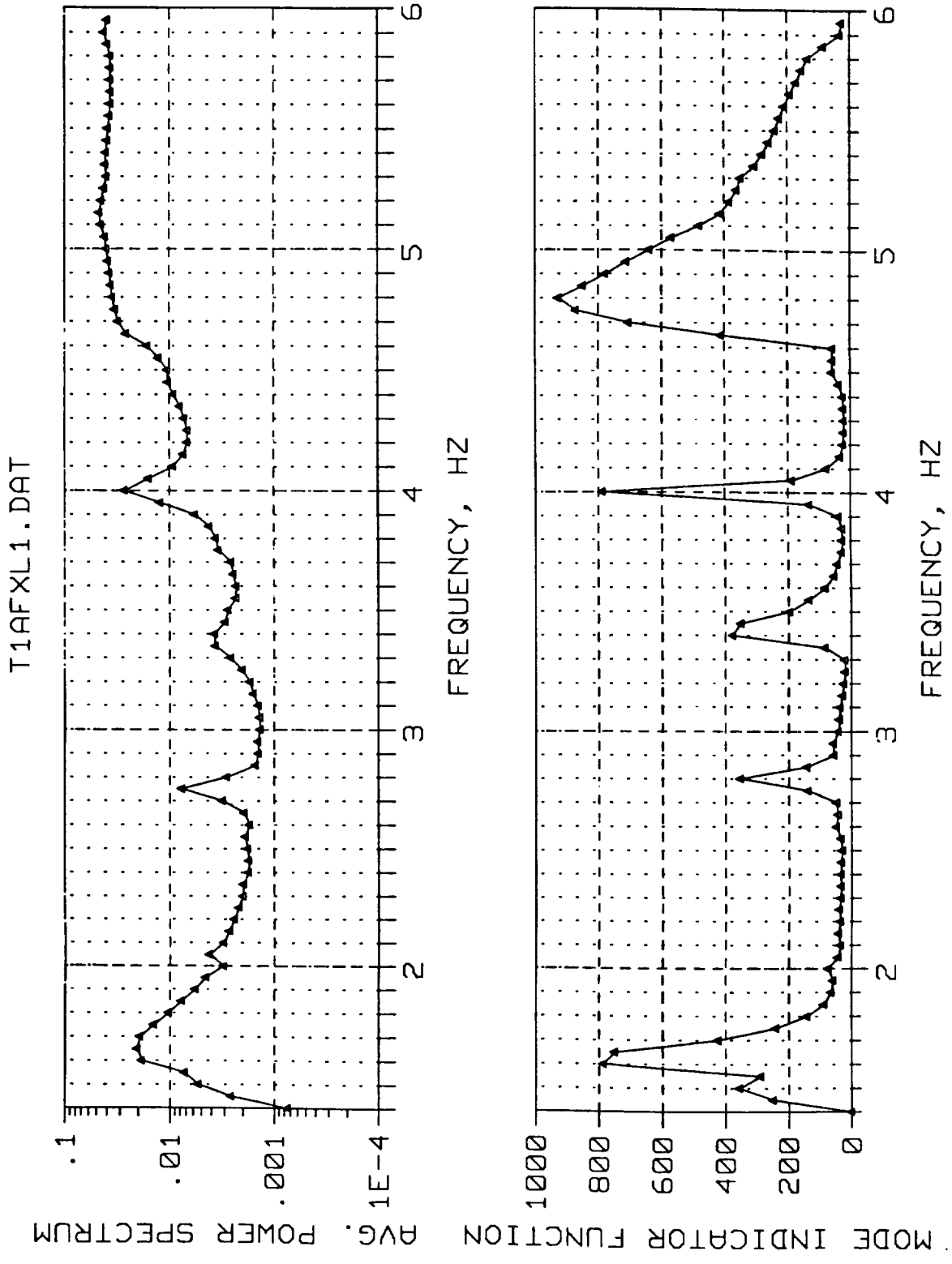

Figure 8. Avg. Power Spectrum and Mode Indicator Function for Test AFXL1

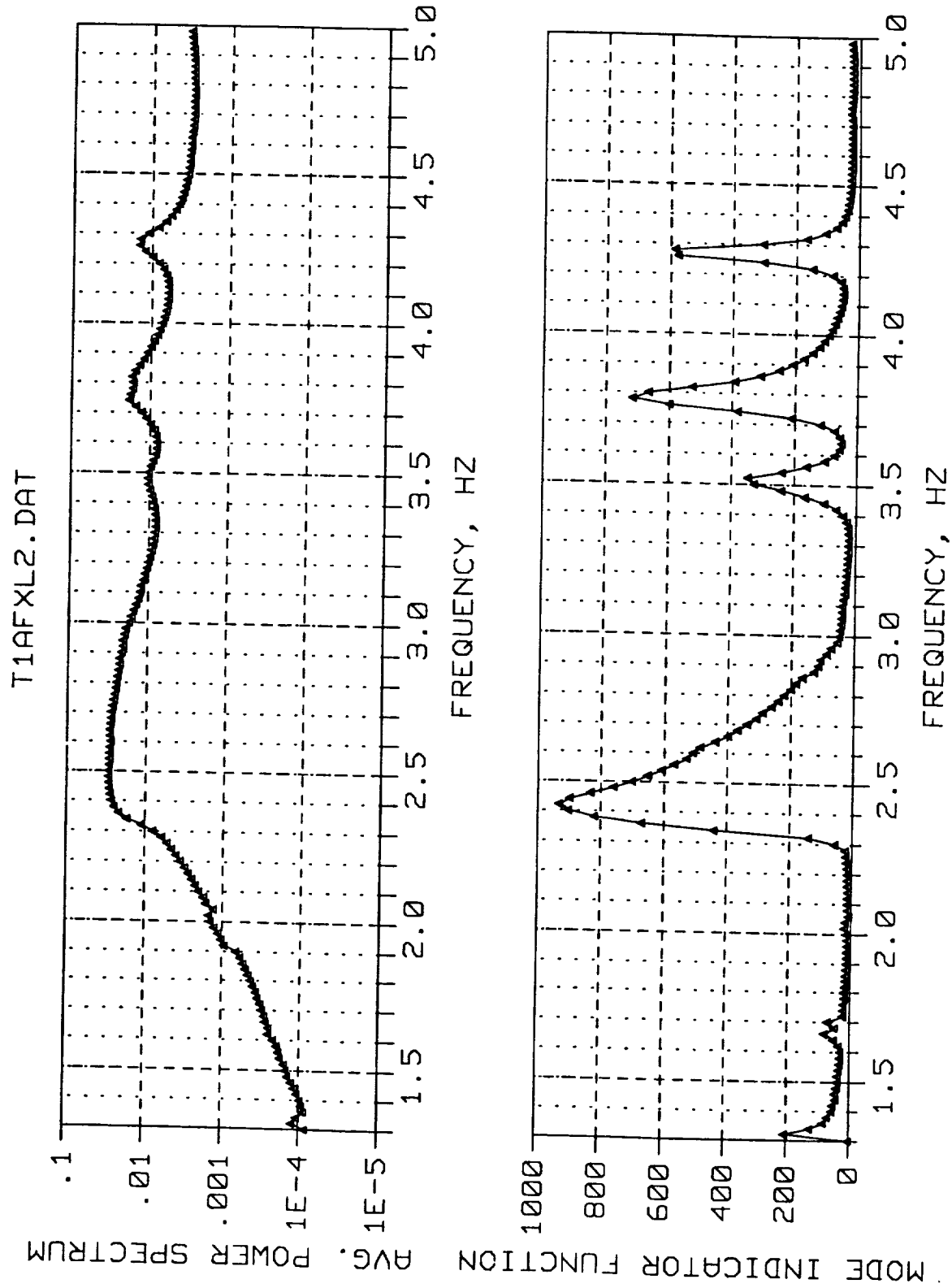

Figure 9. Avg. Power Spectrum and Mode Indicator Function for Test AFXL2

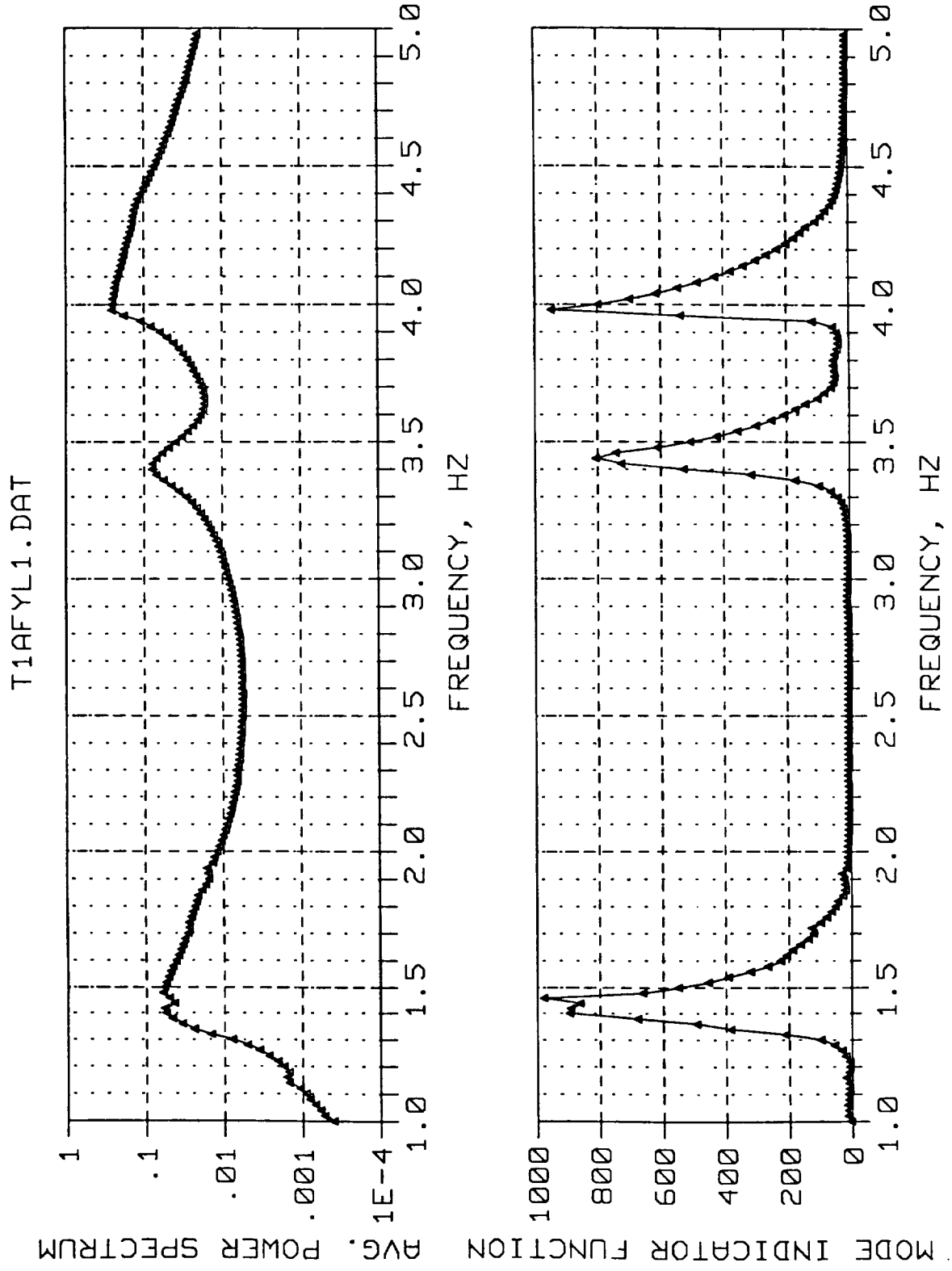

Figure 10. Avg. Power Spectrum and Mode Indicator Function for Test AFYL1

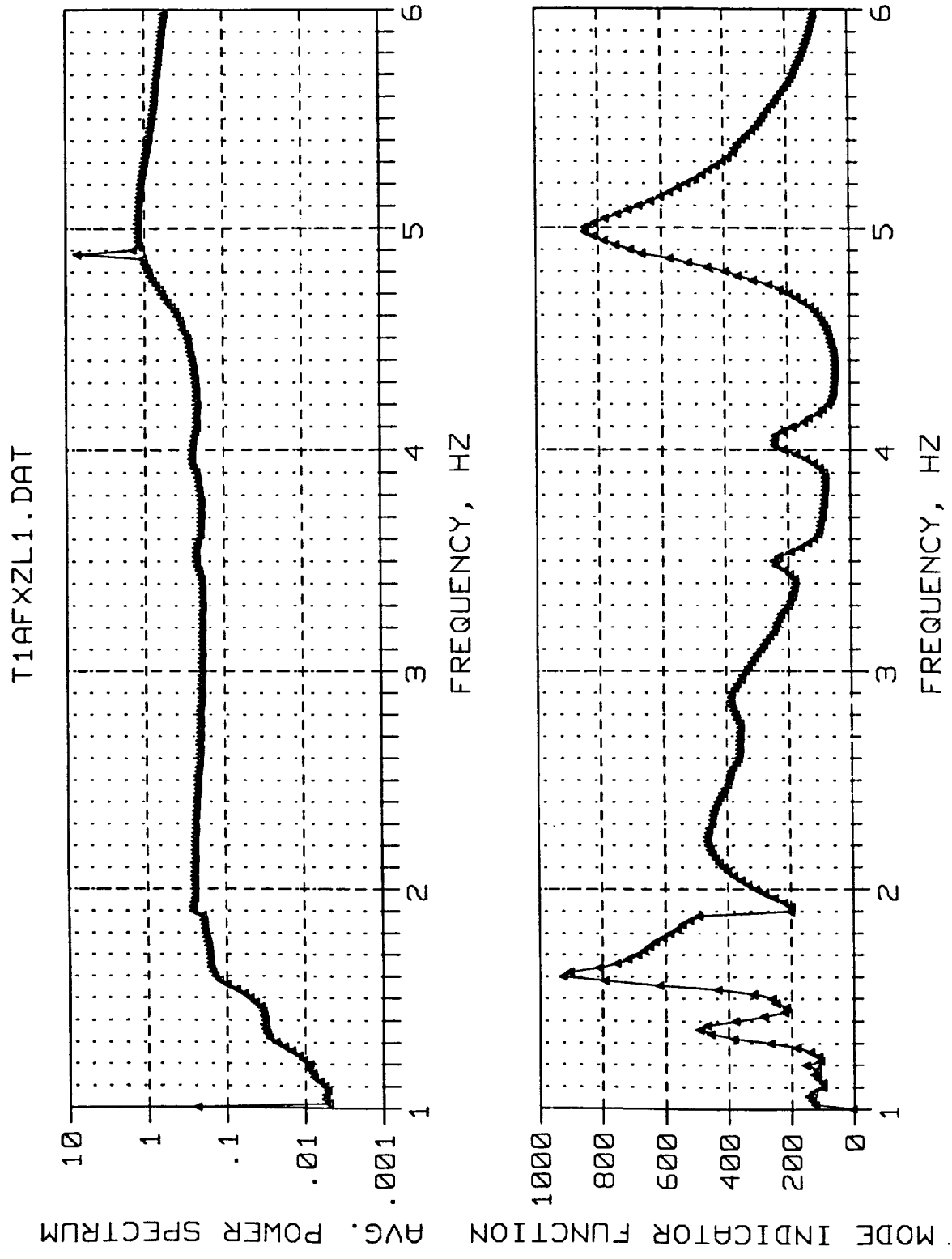

Figure 11. Avg. Power Spectrum and Mode Indicator Function for Test AFXZL1

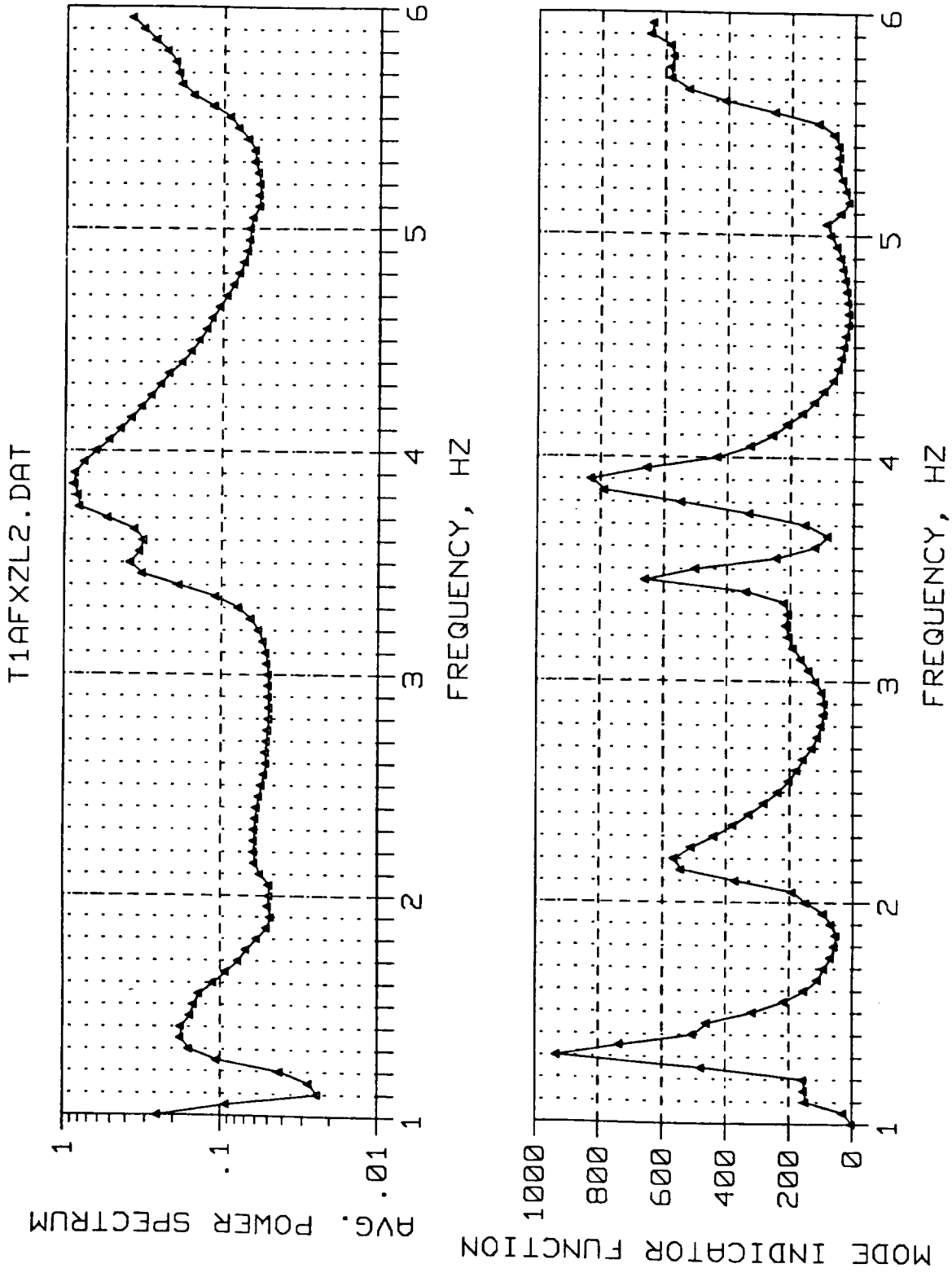

Figure 12. Avg. Power Spectrum and Mode Indicator Function for Test AFXZL2

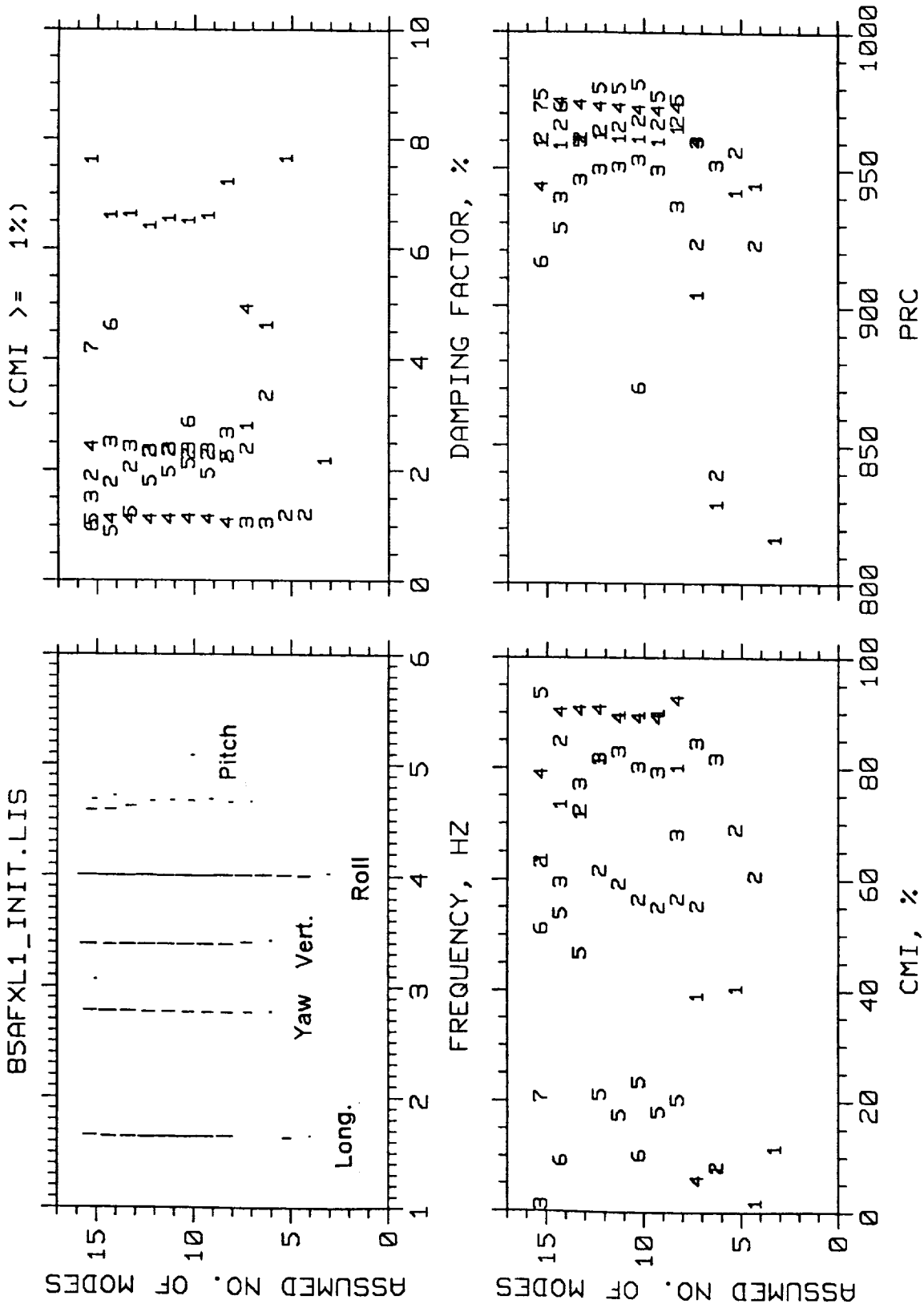

Figure 13a. Initial ERA Results for Test AFXL1

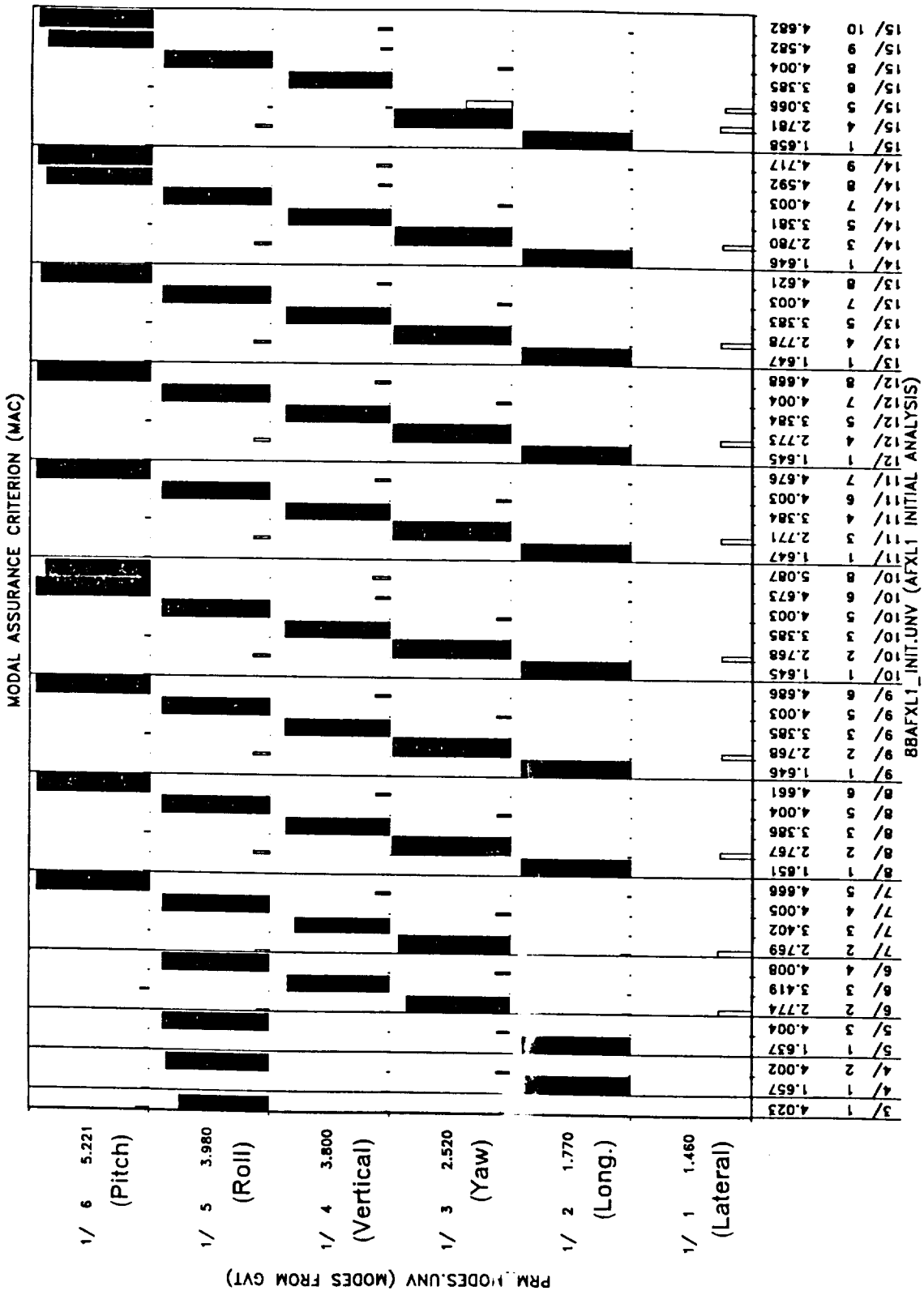

Figure 13b. Correlation of ERA and GVT Modes for Test AFXL1

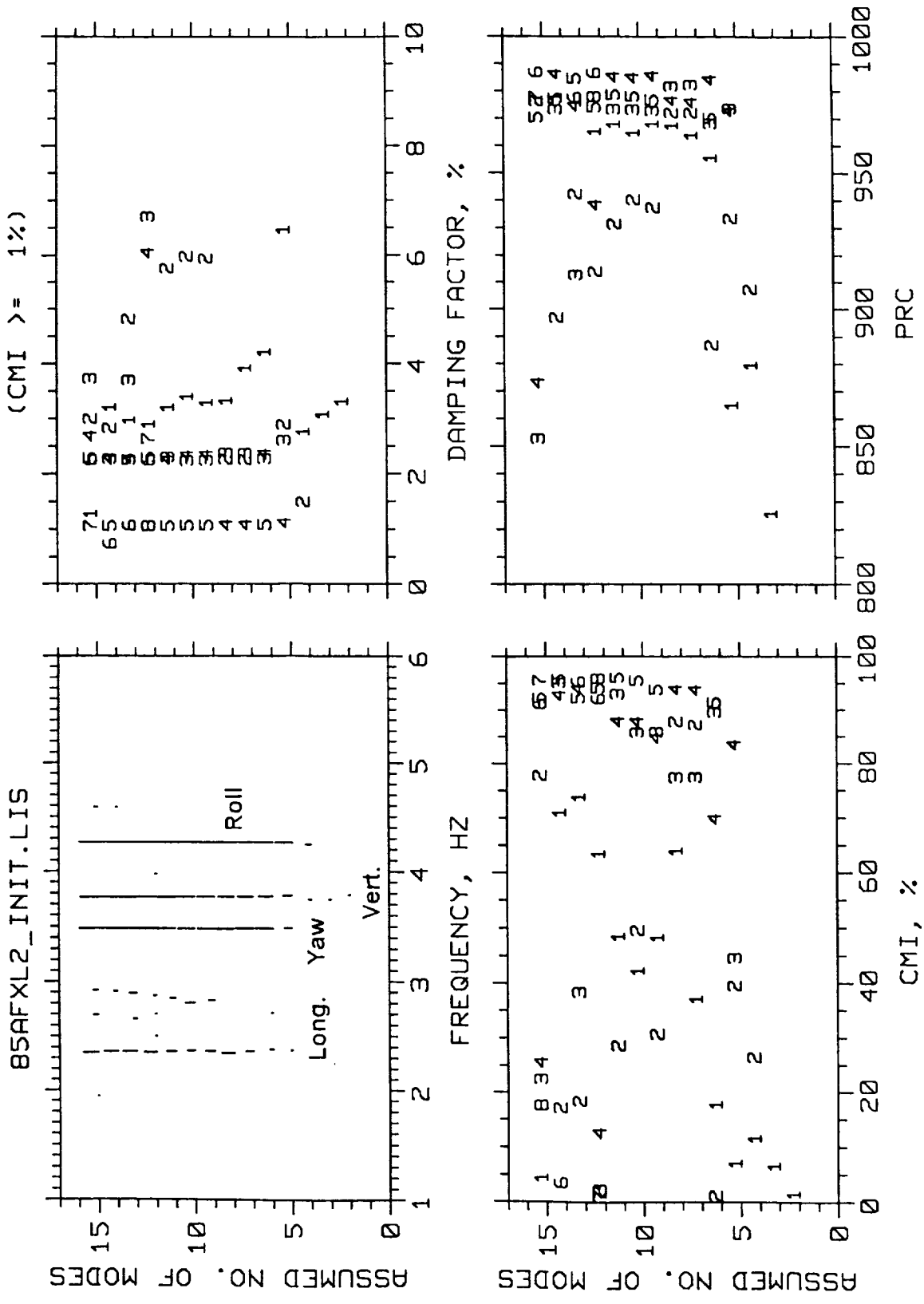

Figure 14a. Initial ERA Results for Test AFXL2

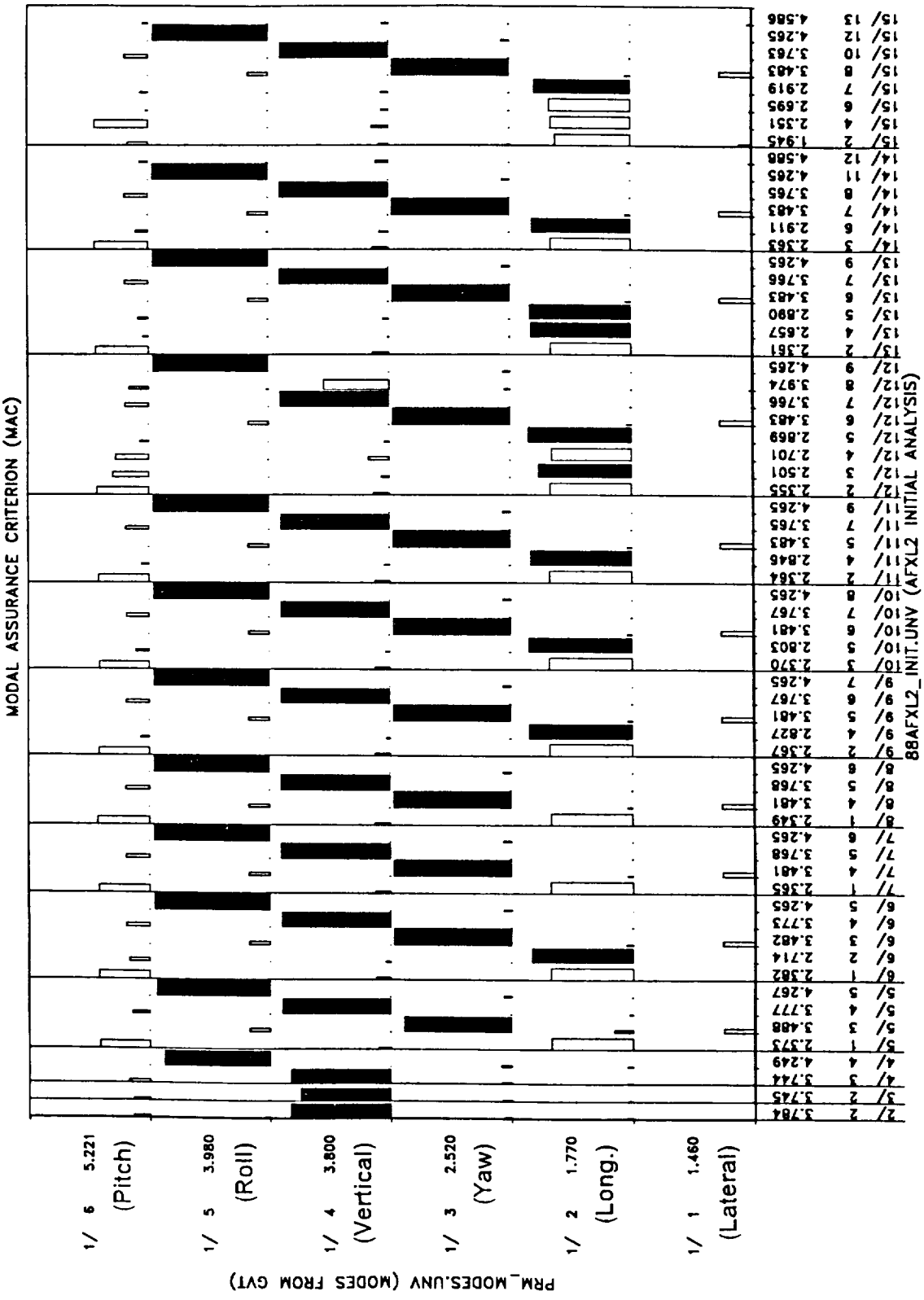

Figure 14b. Correlation of ERA and GVT Modes for Test AFXL2

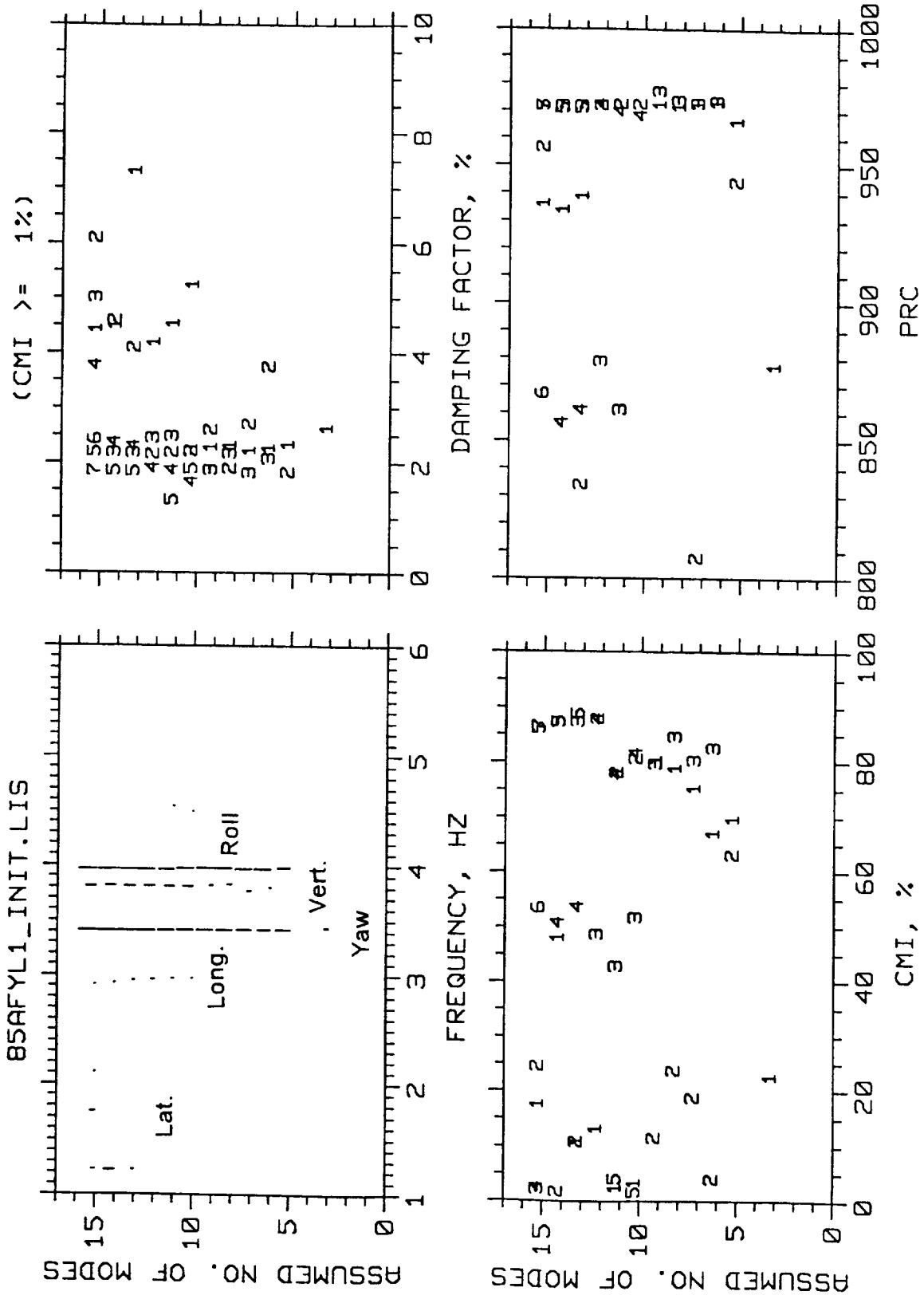

Figure 15a. Initial ERA Results for Test AFYL1

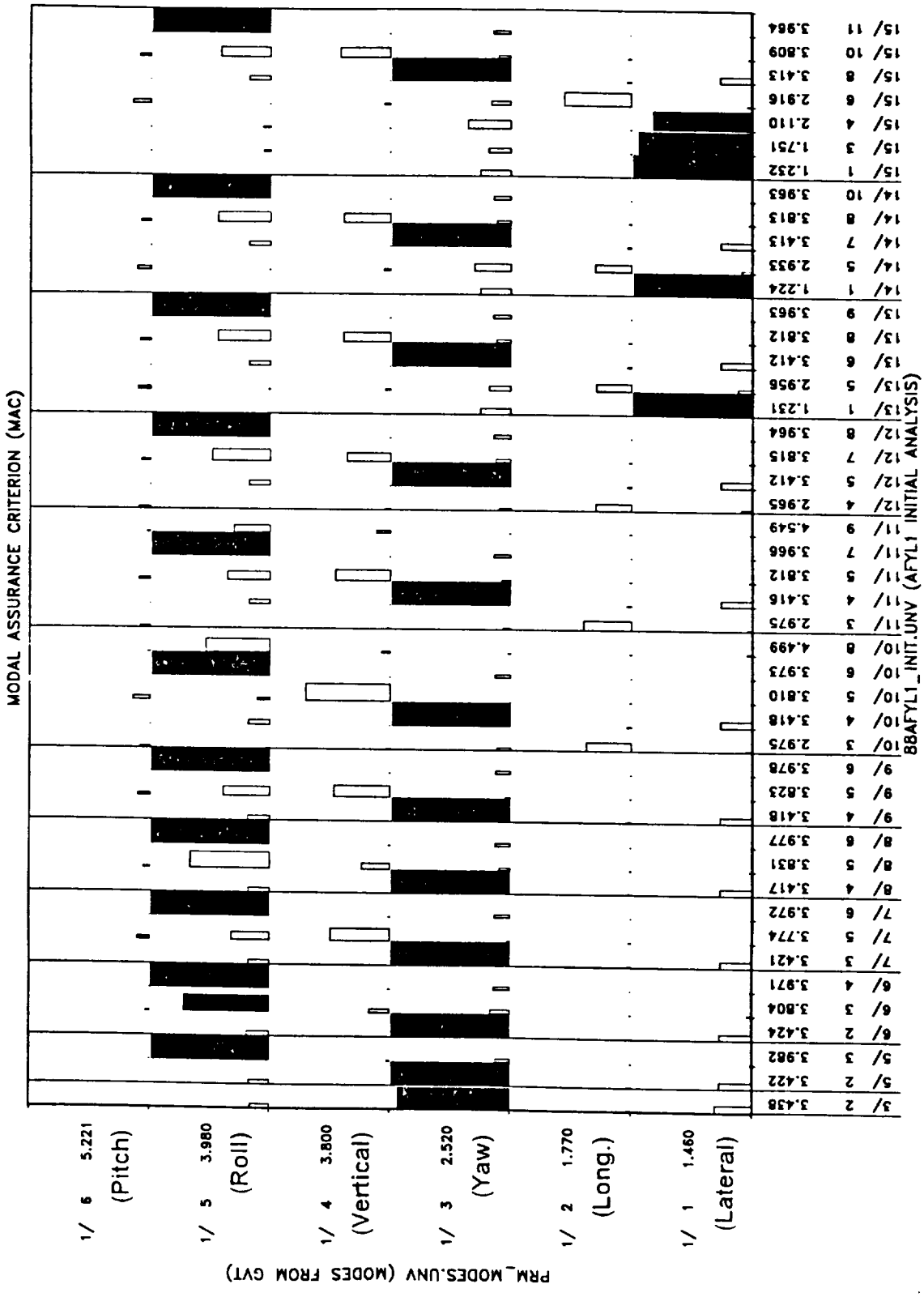

Figure 15b. Correlation of ERA and GVT Modes for Test AFYL1

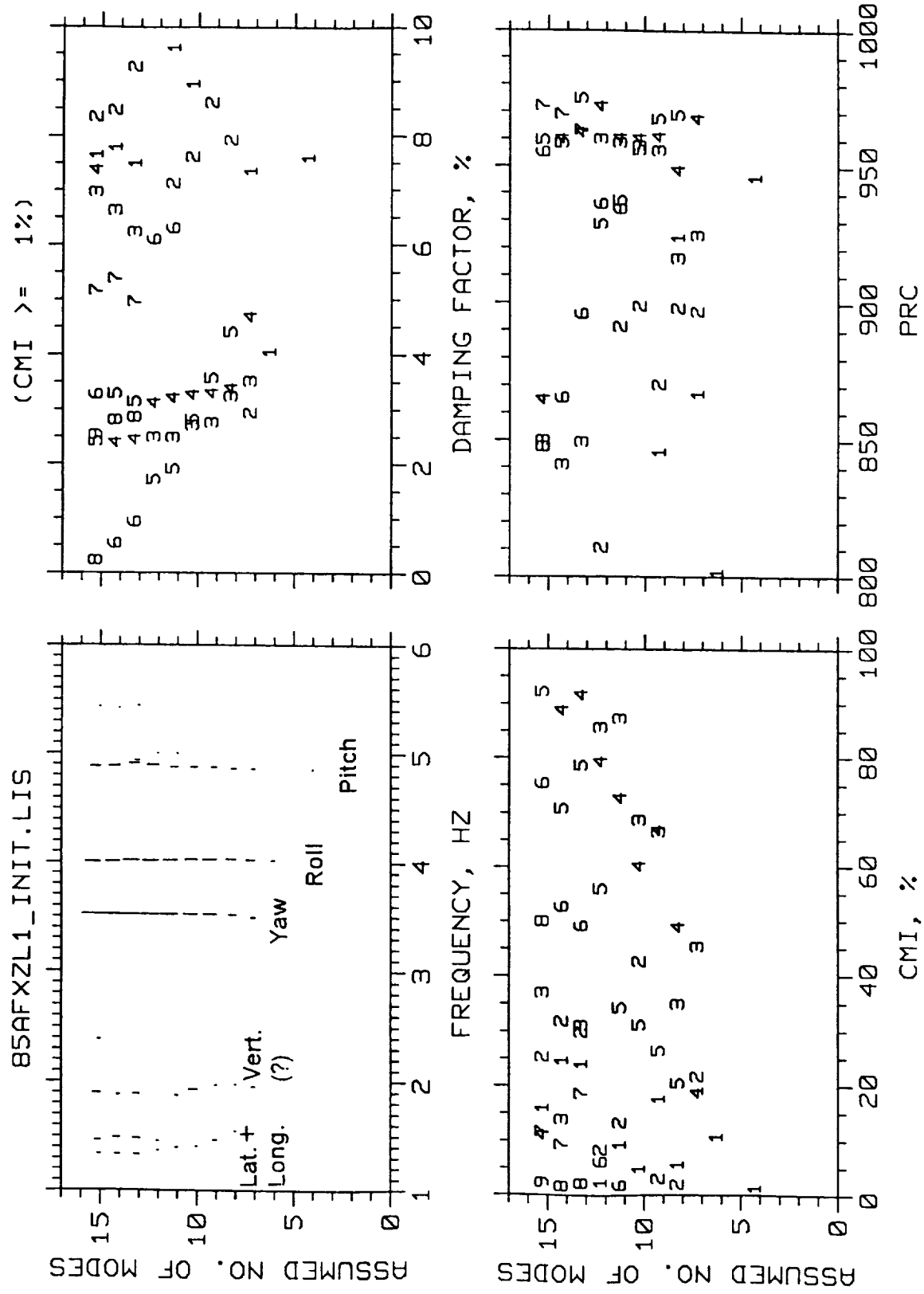

Figure 16a. Initial ERA Results for Test AFXZL1

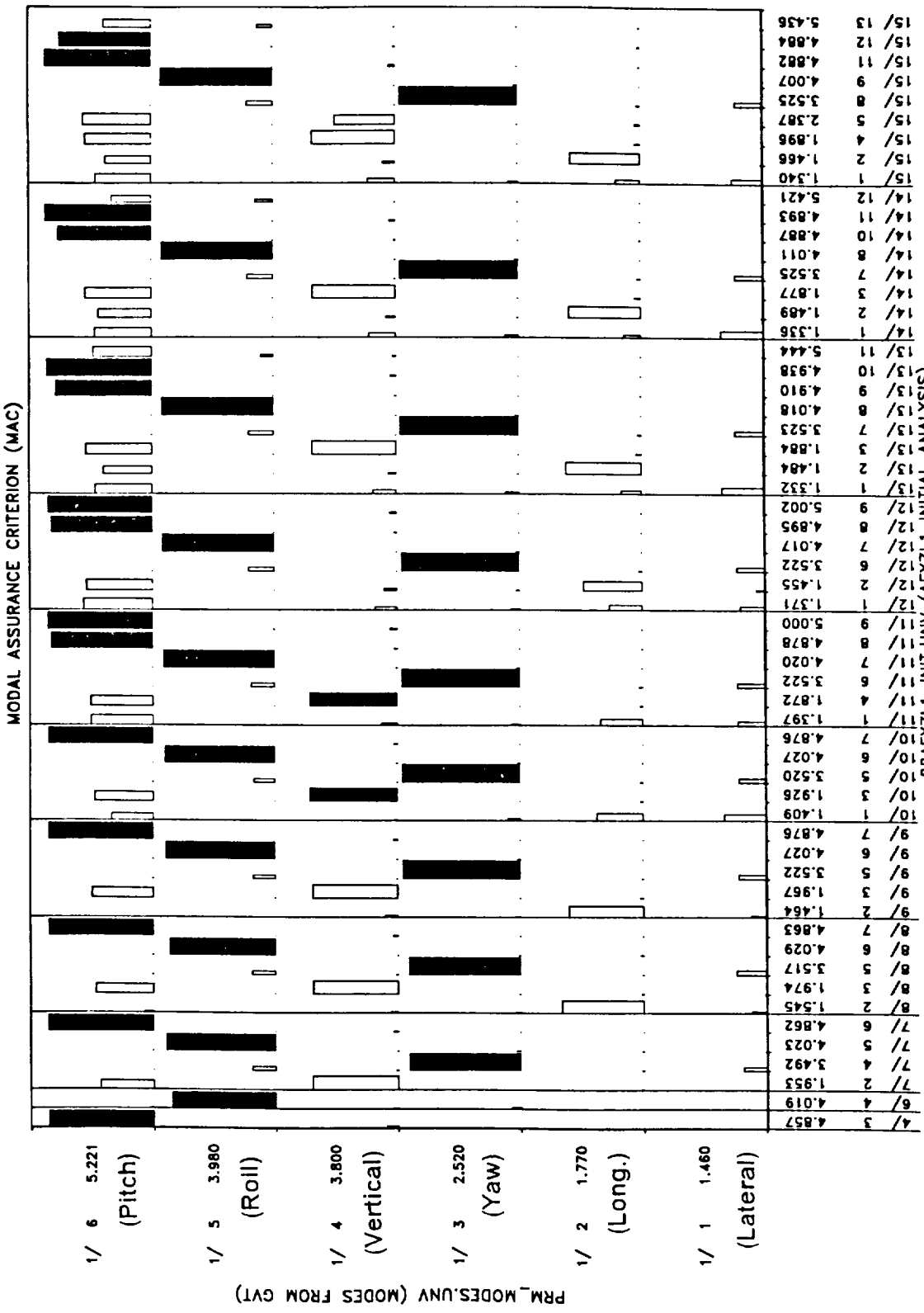

Figure 16b. Correlation of ERA and GVT Modes for Test AFXZL1

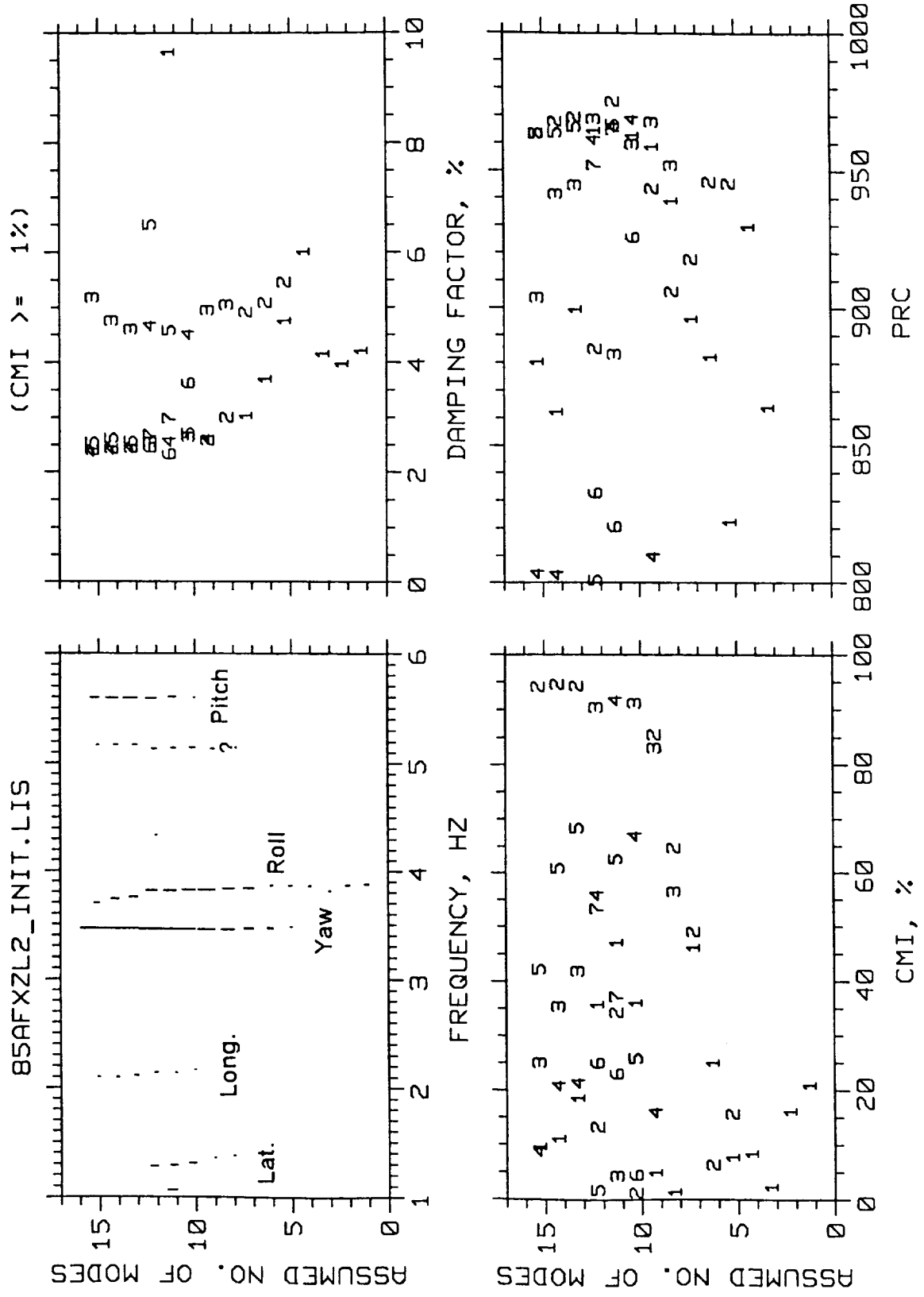

Figure 17a. Initial ERA Results for Test AFXZL2

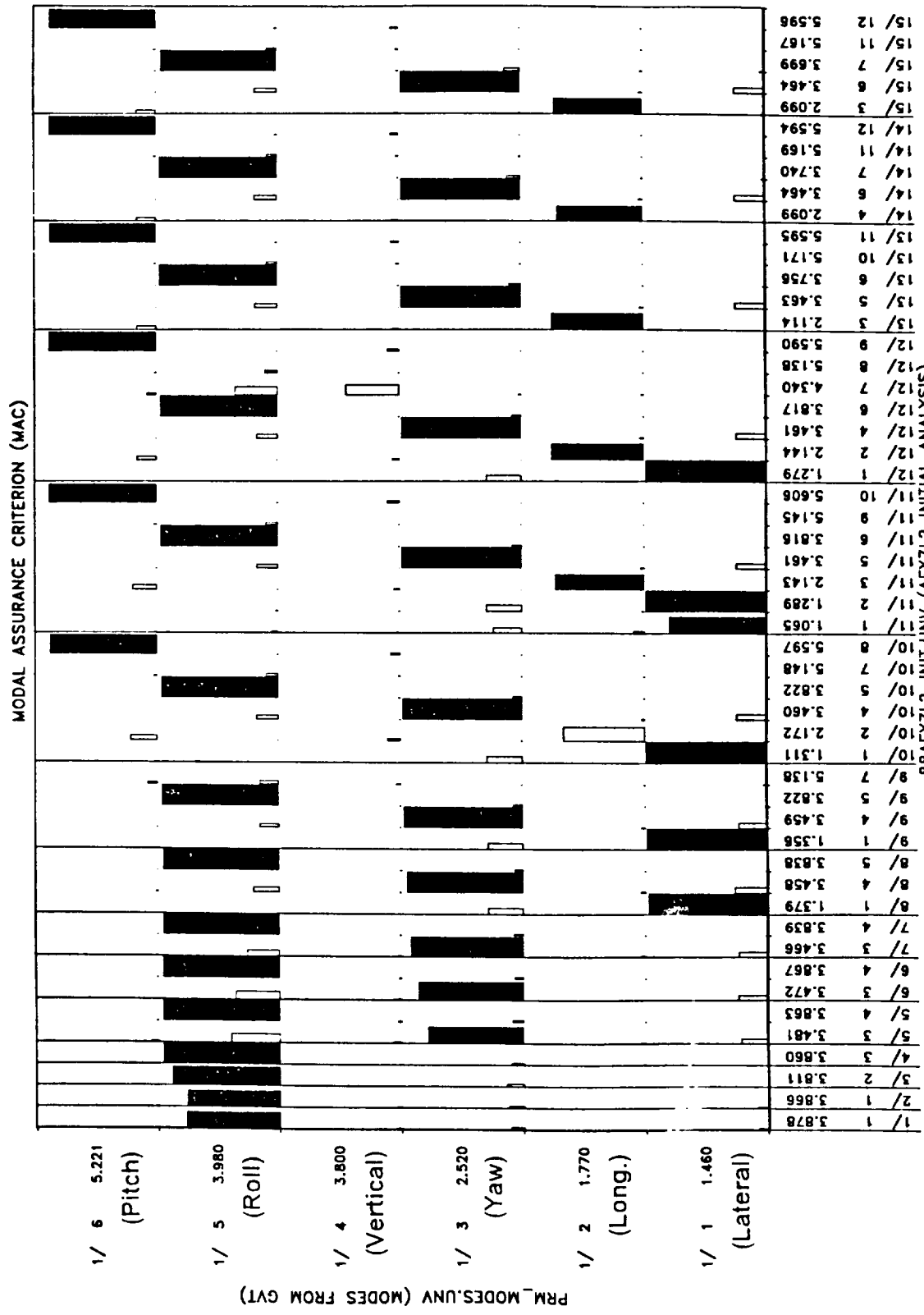

Figure 17b. Correlation of ERA and GVT Modes for Test AFXZL2

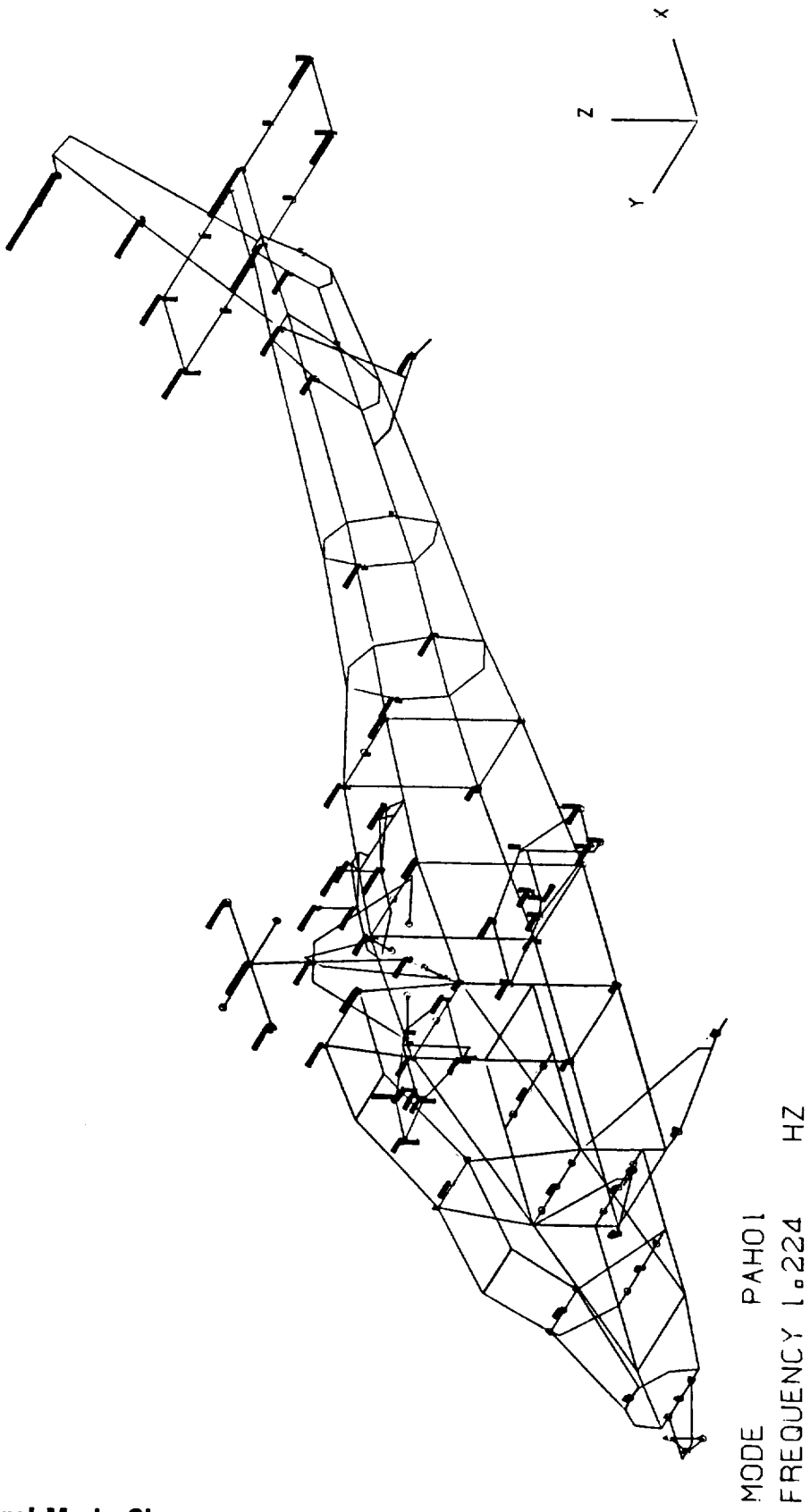

Figure 18. Lateral Mode Shape

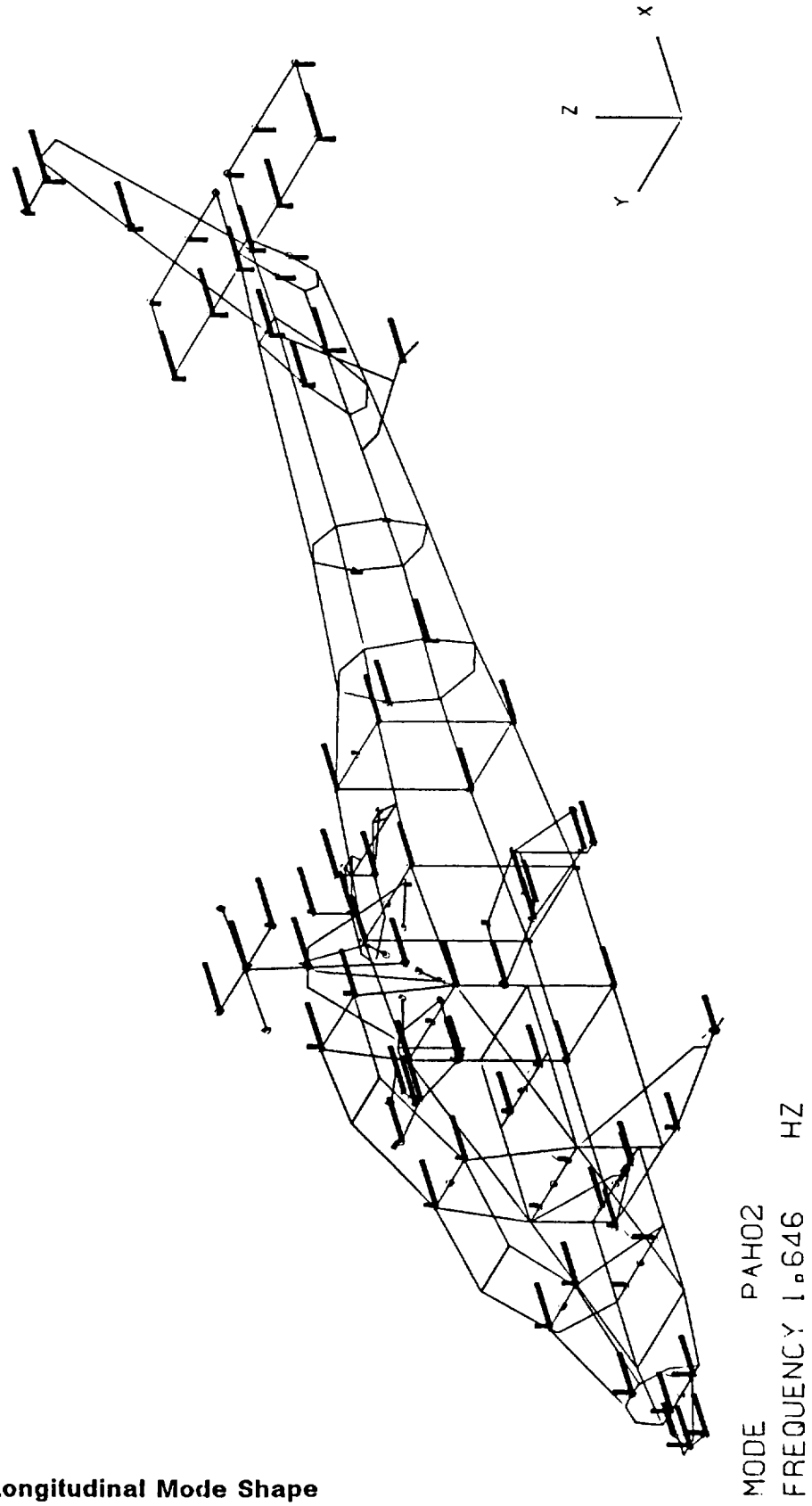

Figure 19. Longitudinal Mode Shape

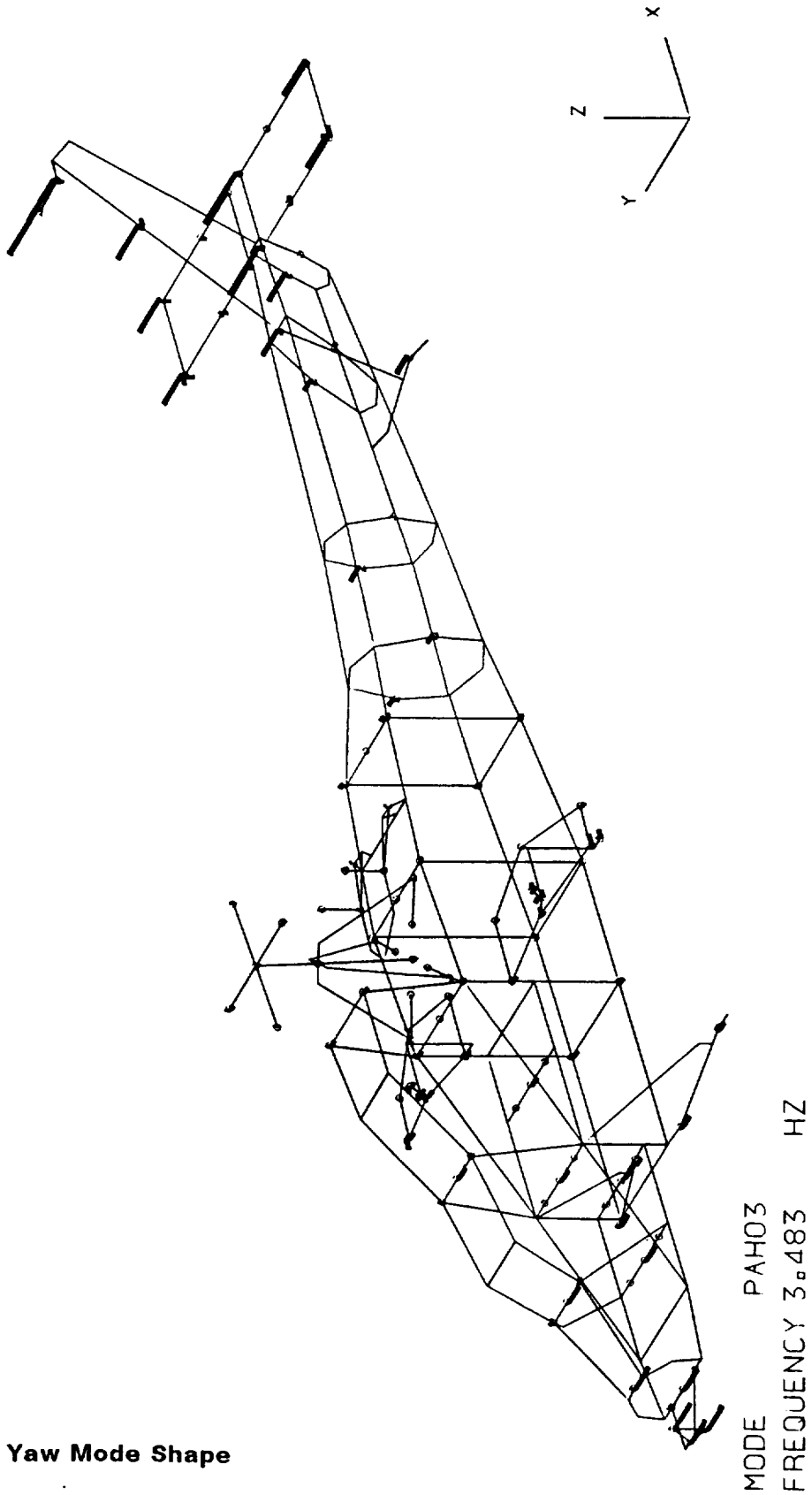

Figure 20. Yaw Mode Shape

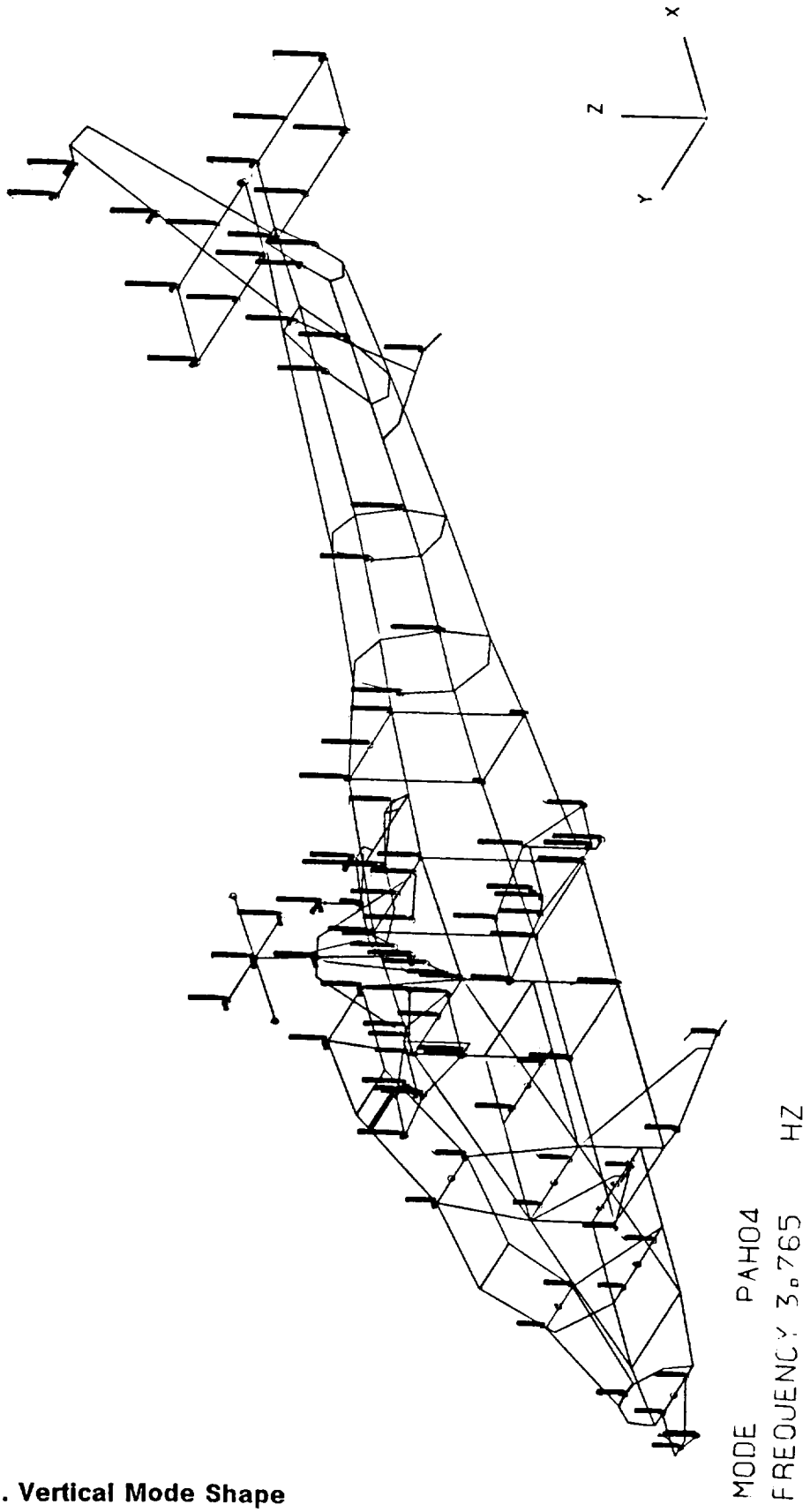

Figure 21. Vertical Mode Shape

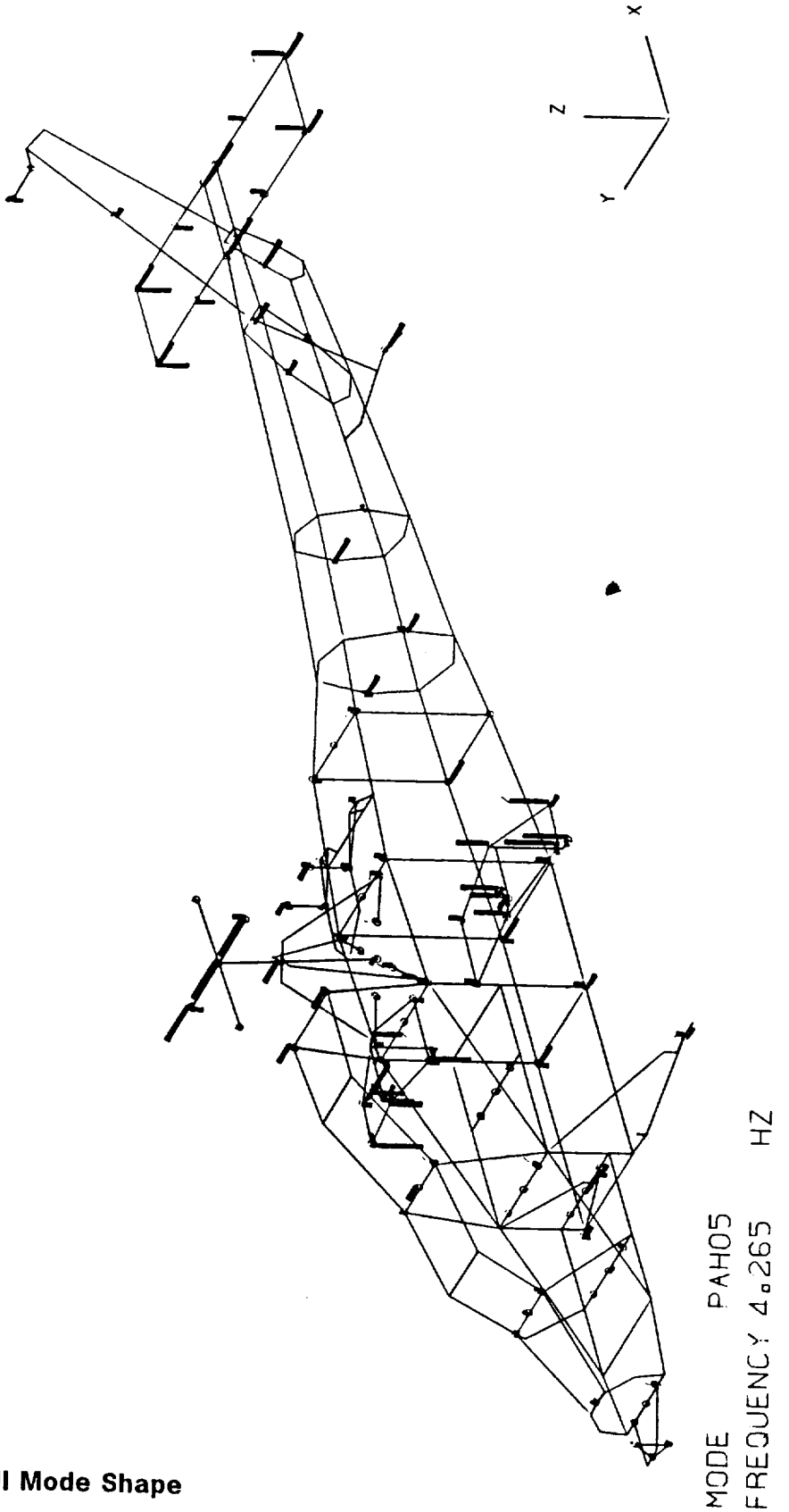

Figure 22. Roll Mode Shape

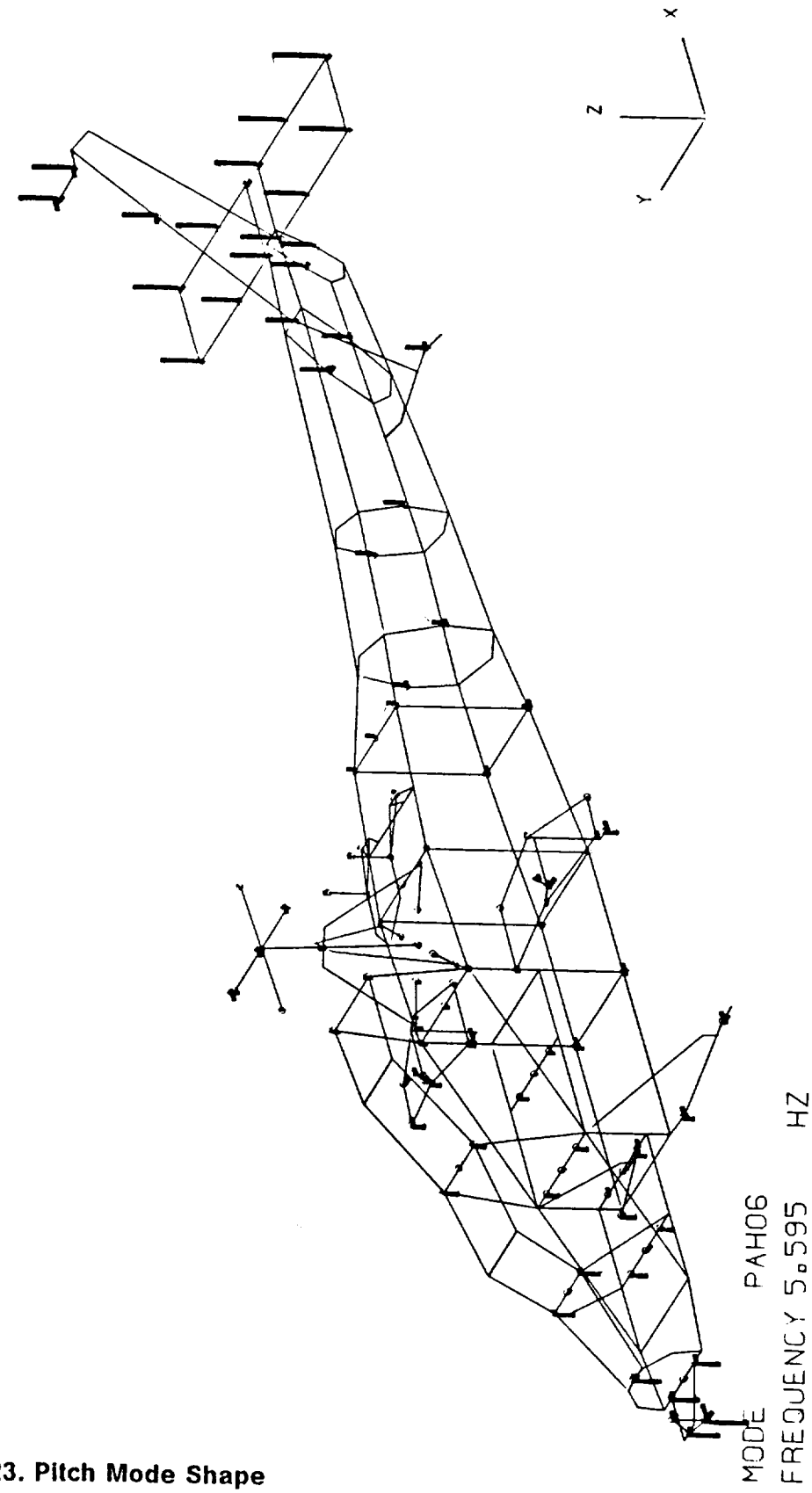

Figure 23. Pitch Mode Shape

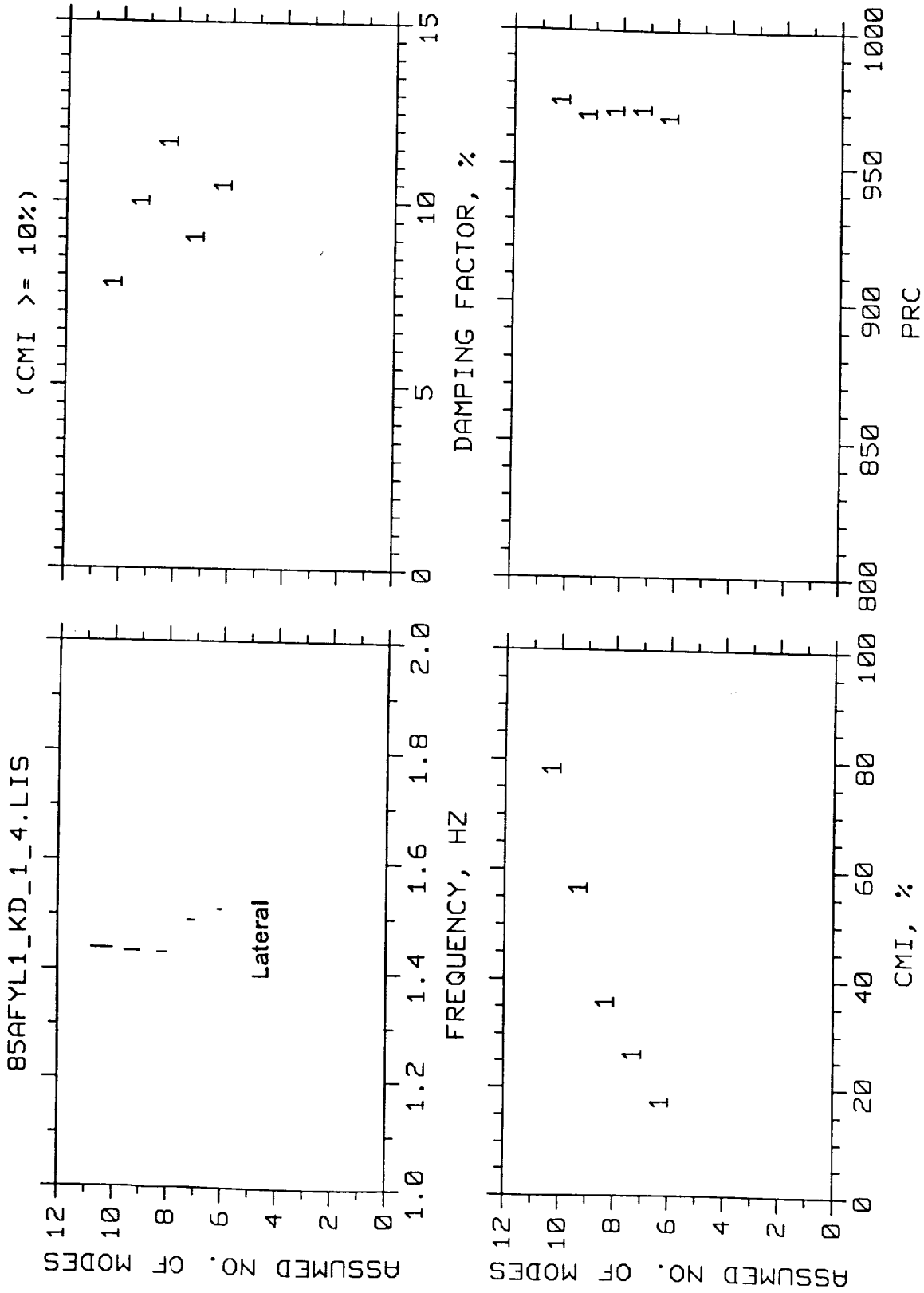

Figure 24. Improved Results for Lateral Mode (Test AFYL1)

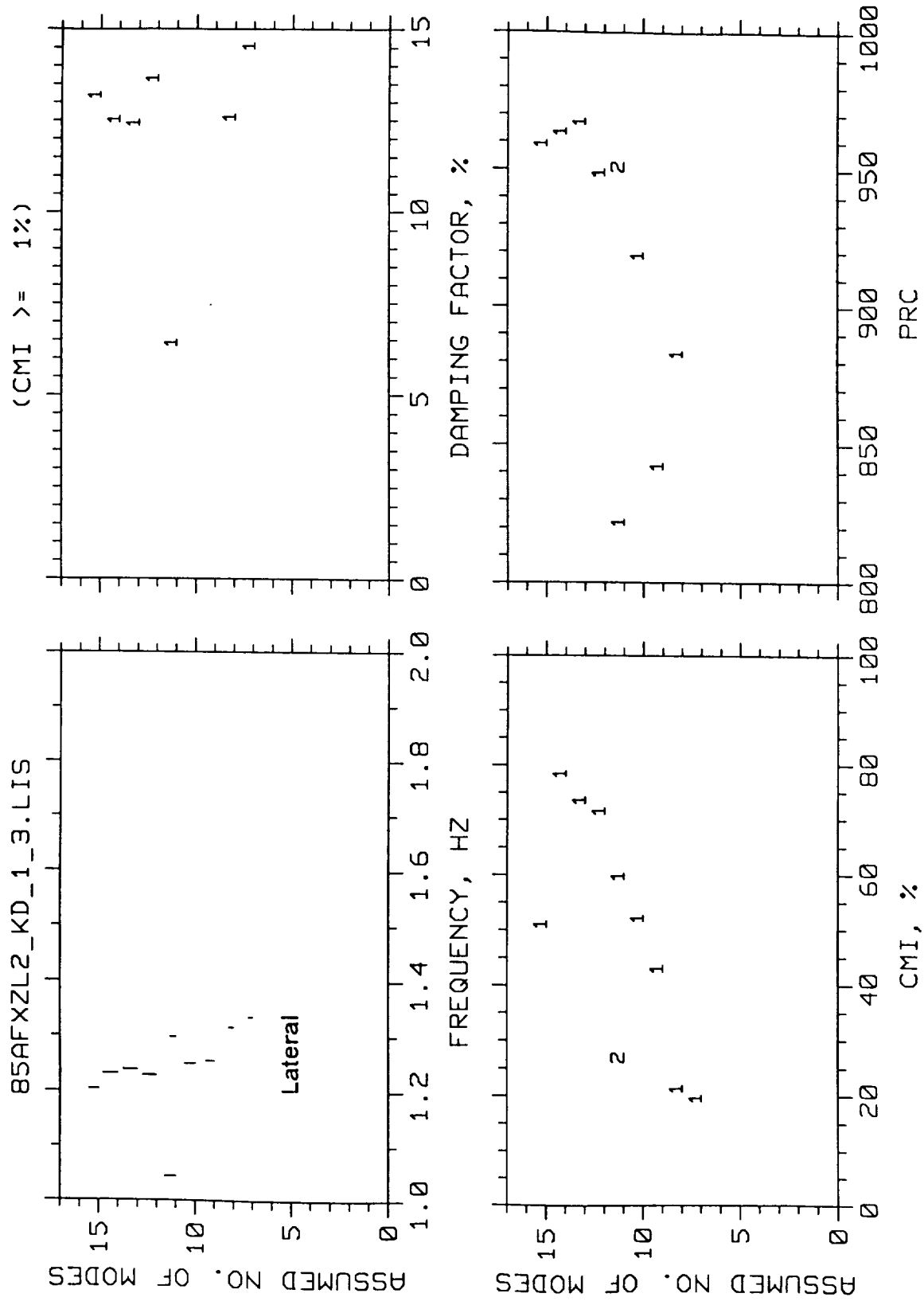

Figure 25. Improved Results for Lateral Mode (Test AFXZL2)

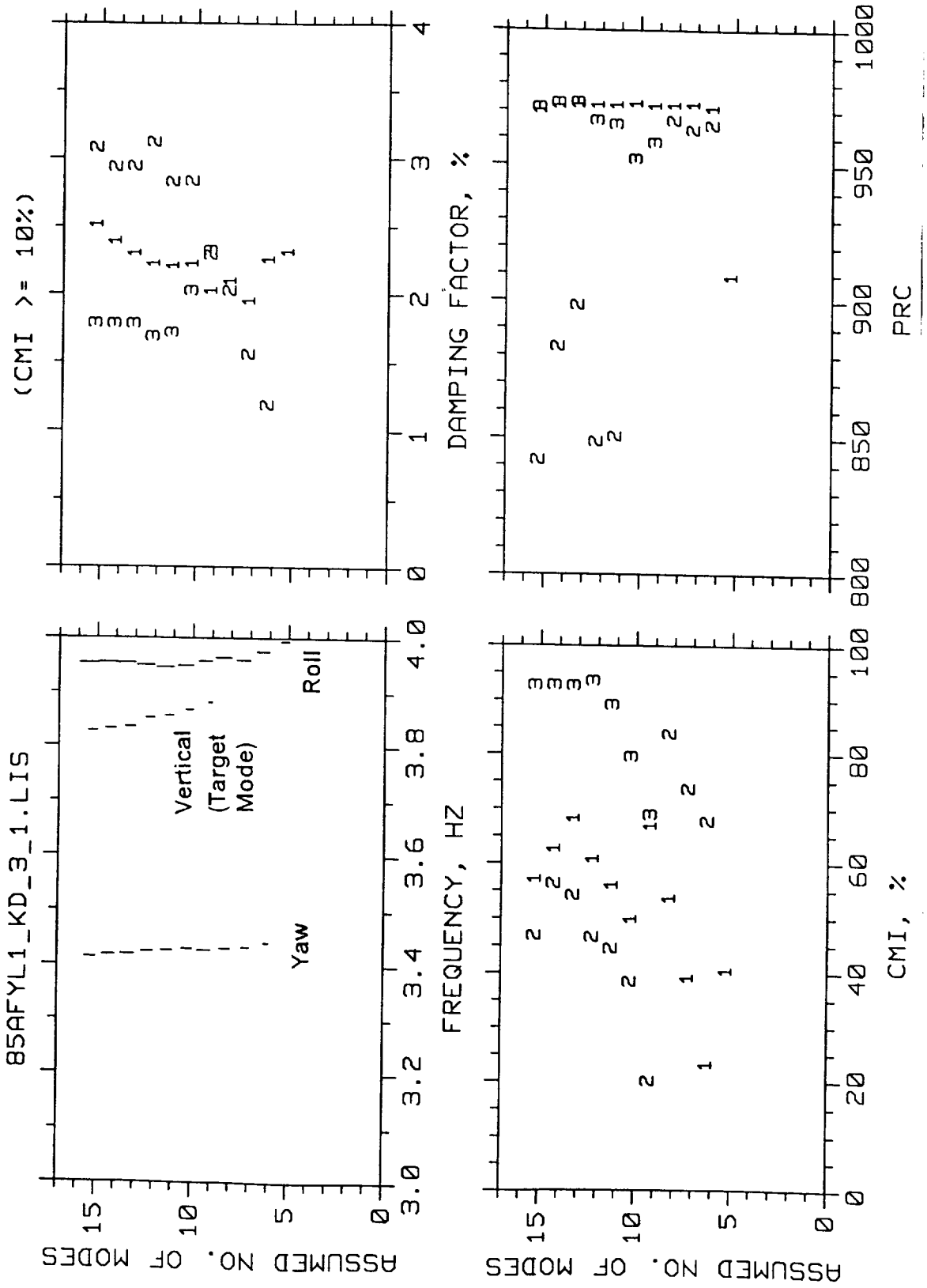

Figure 26. Improved Results for Vertical Mode (Test AFYL1)

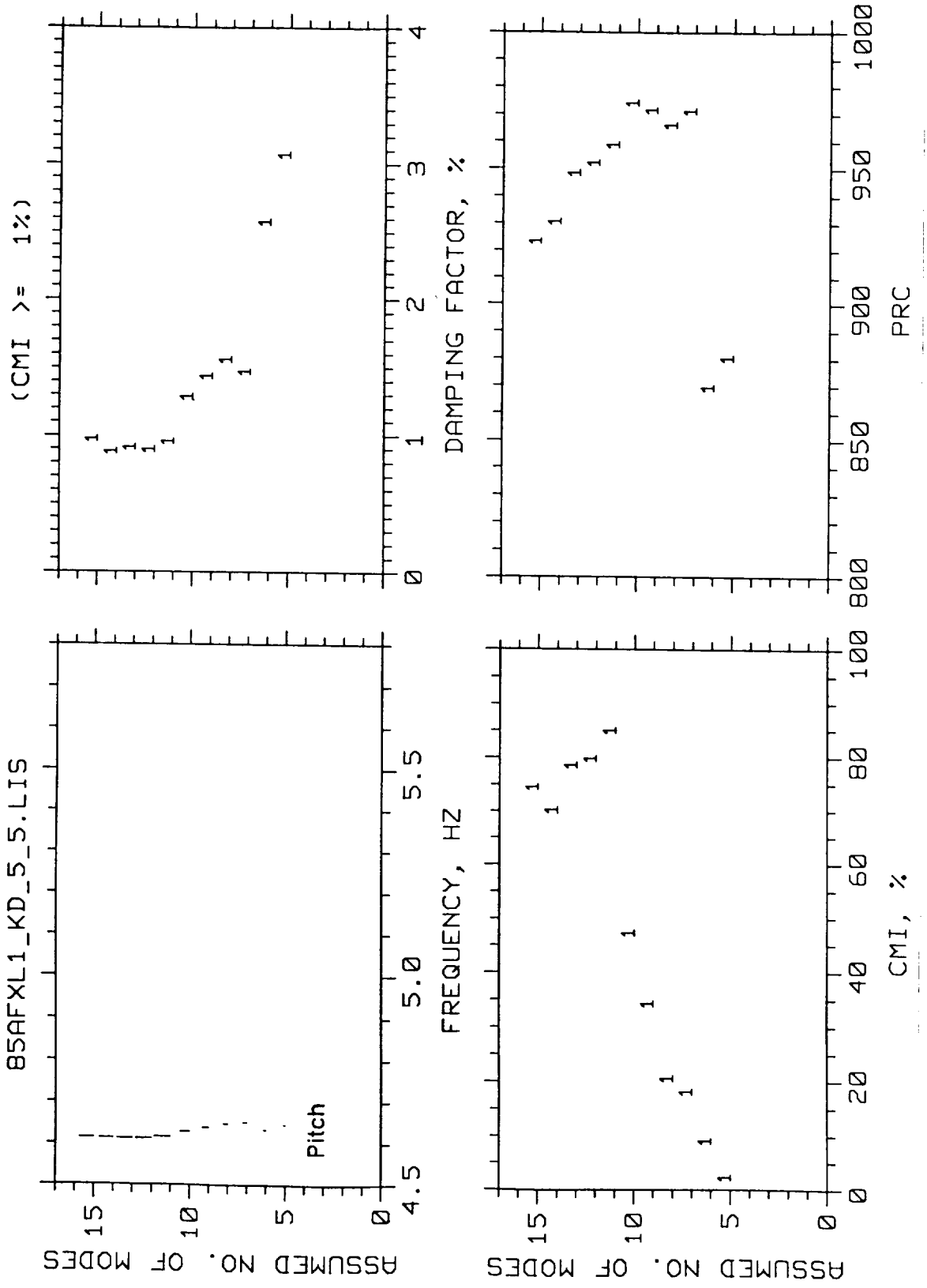

Figure 27. Improved Results for Pitch Mode (Test AFXL1)

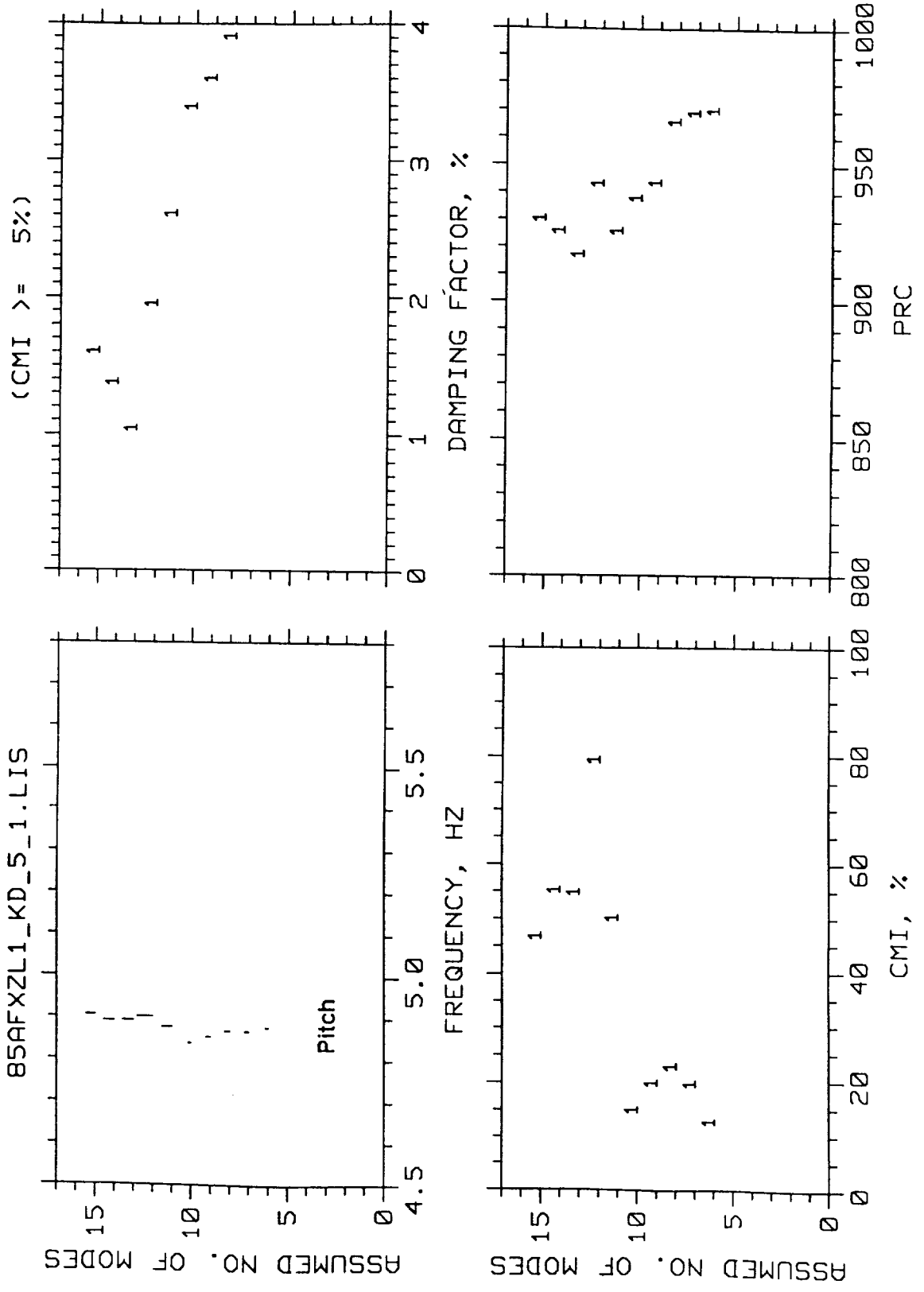

Figure 28. Improved Results for Pitch Mode (Test AFXZL1)

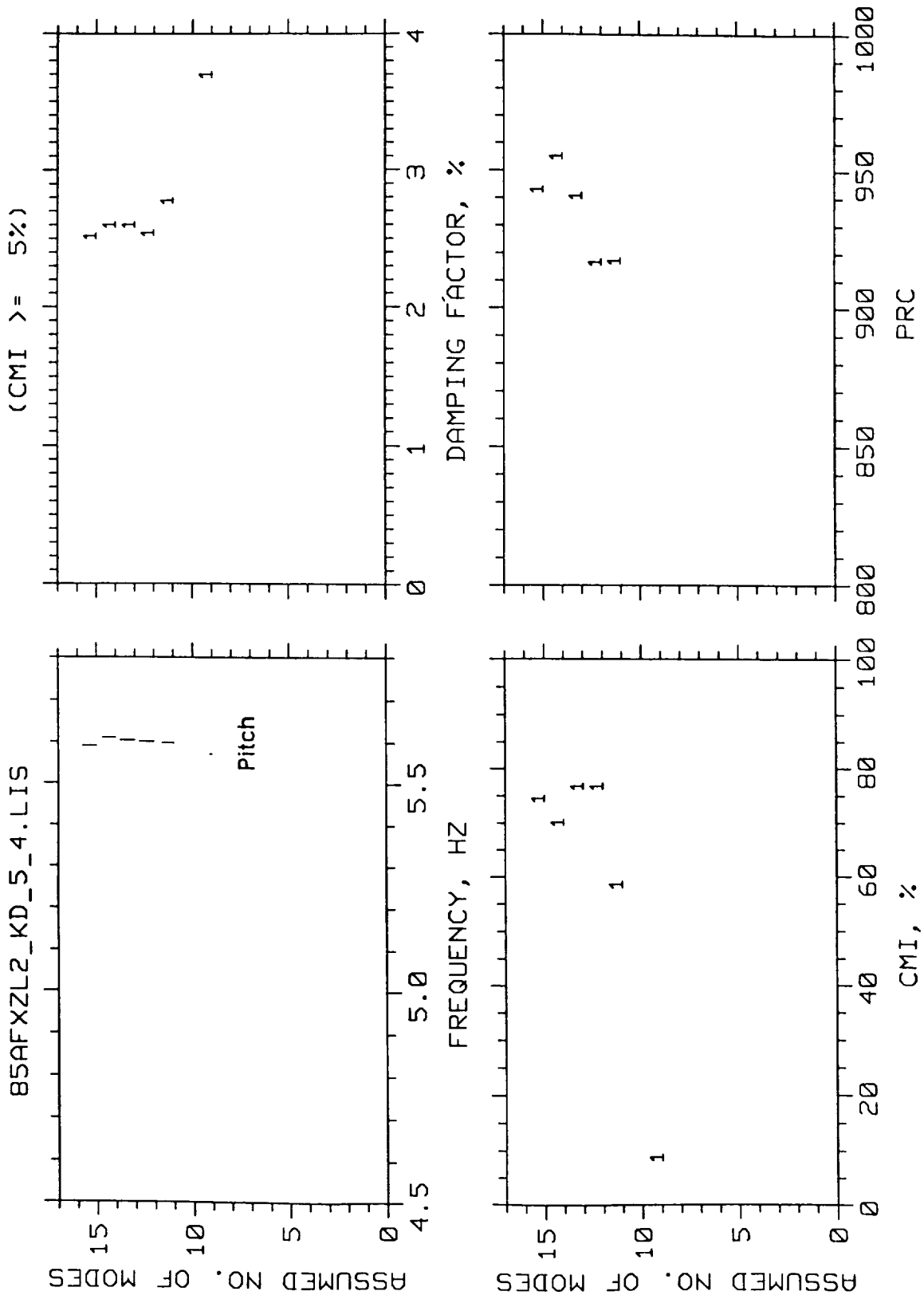

Figure 29. Improved Results for Pitch Mode (Test AFXZL2)

REPORT DOCUMENTATION PAGE

Form Approved
OMB No. 0704-0188

1. AGENCY USE ONLY (Leave blank)	2. REPORT DATE	3. REPORT TYPE AND DATES COVERED
	October 1992	Technical Memorandum

4. TITLE AND SUBTITLE
Rigid Mode Body Identification of the PAH-2 Helicopter Using the Eigensystem Realization Algorithm

5. FUNDING NUMBERS
WU 590-14-61-01

6. AUTHOR(S)
Axel Schenk and Richard S. Pappa

7. PERFORMING ORGANIZATION NAME(S) AND ADDRESS(ES)
NASA Langley Research Center
Hampton, VA 23681-0001

8. PERFORMING ORGANIZATION REPORT NUMBER

9. SPONSORING / MONITORING AGENCY NAME(S) AND ADDRESS(ES)
National Aeronautics and Space Administration
Washington, DC 20546-0001

10. SPONSORING / MONITORING AGENCY REPORT NUMBER
NASA TM-107690

11. SUPPLEMENTARY NOTES
Schenk: DLR Institute of Aeroelasticity, Göttingen, Germany; Pappa: Langley Research Center, Hampton, Virginia. Published also as DLR Report IB 232 - 91007, Nov. 1991. Work performed under a collaborative research agreement in Dynamics and Control of Large Space Systems.

12a. DISTRIBUTION / AVAILABILITY STATEMENT
Unclassified - Unlimited

Subject Category 39

12b. DISTRIBUTION CODE

13. ABSTRACT *(Maximum 200 words)*

The rigid body modes of the PAH-2 'Tiger' helicopter were identified using the Eigensystem Realization Algorithm (ERA). This work complements ground vibration tests performed using DLR's traditional phase resonance technique and ISSPA. Rigid body modal parameters are important for ground resonance prediction. Time-domain data for ERA were obtained by inverse Fourier transformation of frequency response functions measured with stepped-sine excitation. Mode purity (based on the Phase Resonance Criterion) was generally equal to or greater than correponding results obtained in the ground vibration tests. All identified natural frequencies and mode shapes correlate well with corresponding ground vibration test results.

The modal identification approach discussed in this report has become increasingly attractive in recent years due to the steadily declining cost and increased performance of scientific computers. As illustrated in this application, modern time-domain methods can be successfully applied to data acquired using DLR's existing test equipment. Some suggestions are made for future applications of time domain modal identification in this manner.

14. SUBJECT TERMS	15. NUMBER OF PAGES
PAH-2 Tiger Helicopter Modal Identification Eigensystem Realization Algorithm	51
	16. PRICE CODE A04

17. SECURITY CLASSIFICATION OF REPORT	18. SECURITY CLASSIFICATION OF THIS PAGE	19. SECURITY CLASSIFICATION OF ABSTRACT	20. LIMITATION OF ABSTRACT
Unclassified	Unclassified	Unclassified	